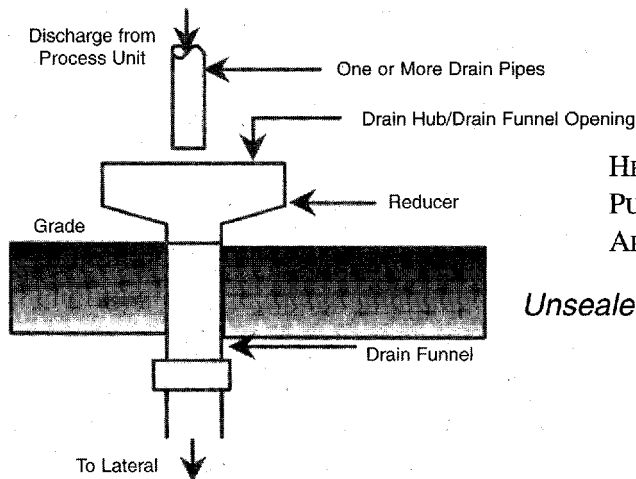
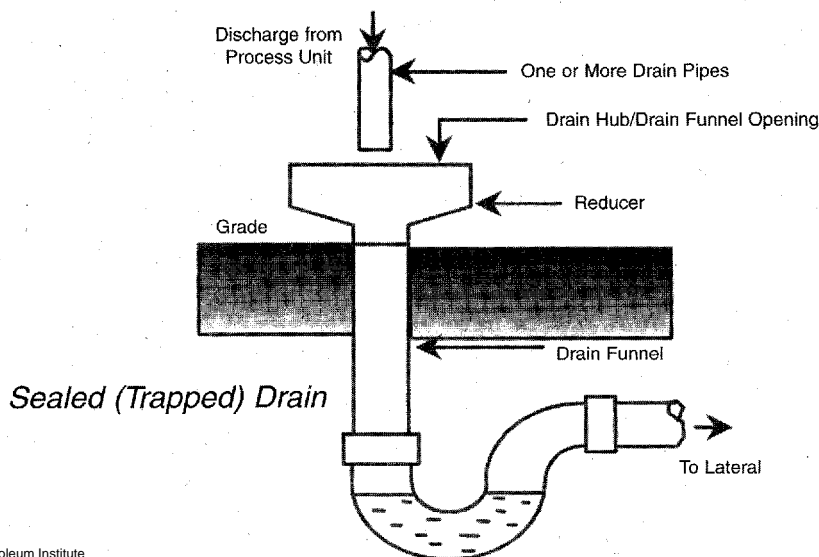


# FUGITIVE EMISSIONS FROM REFINERY PROCESS DRAINS VOLUME II

## FUNDAMENTALS OF FUGITIVE EMISSIONS FROM REFINERY PROCESS DRAINS



HEALTH AND ENVIRONMENTAL SCIENCES DEPARTMENT  
PUBLICATION NUMBER 4678  
APRIL 1999



# American Petroleum Institute Environmental, Health, and Safety Mission and Guiding Principles

---

## MISSION

*The members of the American Petroleum Institute are dedicated to continuous efforts to improve the compatibility of our operations with the environment while economically developing energy resources and supplying high quality products and services to consumers. We recognize our responsibility to work with the public, the government, and others to develop and to use natural resources in an environmentally sound manner while protecting the health and safety of our employees and the public. To meet these responsibilities, API members pledge to manage our businesses according to the following principles using sound science to prioritize risks and to implement cost-effective management practices:*

---

## PRINCIPLES

- To recognize and to respond to community concerns about our raw materials, products and operations.
  - To operate our plants and facilities, and to handle our raw materials and products in a manner that protects the environment, and the safety and health of our employees and the public.
  - To make safety, health and environmental considerations a priority in our planning, and our development of new products and processes.
  - To advise promptly, appropriate officials, employees, customers and the public of information on significant industry-related safety, health and environmental hazards, and to recommend protective measures.
  - To counsel customers, transporters and others in the safe use, transportation and disposal of our raw materials, products and waste materials.
  - To economically develop and produce natural resources and to conserve those resources by using energy efficiently.
  - To extend knowledge by conducting or supporting research on the safety, health and environmental effects of our raw materials, products, processes and waste materials.
  - To commit to reduce overall emission and waste generation.
  - To work with others to resolve problems created by handling and disposal of hazardous substances from our operations.
  - To participate with government and others in creating responsible laws, regulations and standards to safeguard the community, workplace and environment.
  - To promote these principles and practices by sharing experiences and offering assistance to others who produce, handle, use, transport or dispose of similar raw materials, petroleum products and wastes.
-

# **Fugitive Emissions From Refinery Process Drains Volume II**

## **Fundamentals of Fugitive Emissions From Refinery Process Drains**

**Health and Environmental Sciences Department**

API PUBLICATION NUMBER 4678

PREPARED UNDER CONTRACT BY:

BROWN AND CALDWELL  
100 WEST HARRISON STREET  
SEATTLE, WASHINGTON 98119-4186

RICHARD L. CORSI  
THE UNIVERSITY OF TEXAS AT AUSTIN  
AUSTIN, TEXAS

APRIL 1999



## FOREWORD

API PUBLICATIONS NECESSARILY ADDRESS PROBLEMS OF A GENERAL NATURE. WITH RESPECT TO PARTICULAR CIRCUMSTANCES, LOCAL, STATE, AND FEDERAL LAWS AND REGULATIONS SHOULD BE REVIEWED.

API IS NOT UNDERTAKING TO MEET THE DUTIES OF EMPLOYERS, MANUFACTURERS, OR SUPPLIERS TO WARN AND PROPERLY TRAIN AND EQUIP THEIR EMPLOYEES, AND OTHERS EXPOSED, CONCERNING HEALTH AND SAFETY RISKS AND PRECAUTIONS, NOR UNDERTAKING THEIR OBLIGATIONS UNDER LOCAL, STATE, OR FEDERAL LAWS.

NOTHING CONTAINED IN ANY API PUBLICATION IS TO BE CONSTRUED AS GRANTING ANY RIGHT, BY IMPLICATION OR OTHERWISE, FOR THE MANUFACTURE, SALE, OR USE OF ANY METHOD, APPARATUS, OR PRODUCT COVERED BY LETTERS PATENT. NEITHER SHOULD ANYTHING CONTAINED IN THE PUBLICATION BE CONSTRUED AS INSURING ANYONE AGAINST LIABILITY FOR INFRINGEMENT OF LETTERS PATENT.

*All rights reserved. No part of this work may be reproduced, stored in a retrieval system, or transmitted by any means, electronic, mechanical, photocopying, recording, or otherwise, without prior written permission from the publisher. Contact the publisher, API Publishing Services, 1220 L Street, N.W., Washington, D.C. 20005.*

Copyright © 1999 American Petroleum Institute

## ACKNOWLEDGMENTS

THE FOLLOWING PEOPLE ARE RECOGNIZED FOR THEIR CONTRIBUTIONS OF TIME AND EXPERTISE DURING THIS STUDY AND IN THE PREPARATION OF THIS REPORT:

### API STAFF CONTACT

Paul Martino, Health and Environmental Sciences Department

### MEMBERS OF THE REFINERY DRAINS EMISSIONS PROJECT GROUP

Nick Spiridakis, Chairman, Chevron Research and Technology

Karel Jelinek, BP Oil Company

Miriam Lev-On, Arco

Gary Morris, Mobil Technology Company

Chris Rabideau, Texaco

Manuel Cano, Shell Development Company

Achar Ramachandra, Amoco Corporation

Jeff Siegell, Exxon Research and Engineering

Ron Wilkniss, Western States Petroleum Association

Jenny Yang, Marathon Oil Company

Brown and Caldwell would also like to thank Dr. Richard Corsi (University of Texas) for his assistance in the completion of this work.

## PREFACE

The results of this study are presented in three separate reports.

- Volume I entitled "*Fugitive Emission Factors for Refinery Process Drains*" (API Publication Number 4677) contains simplified emission factors that can be used to quickly estimate total volatile organic compound (VOC) emissions from refinery process drains.
- Volume II entitled "*Fundamentals of Fugitive Emissions from Refinery Process Drains*" (API Publication Number 4678) describes theoretical concepts and equations that may be used in a model (APIDRAIN) to estimate speciated VOC emissions. The model can provide insight on how to change process drain variables (flow rate, temperature, etc.) to reduce emissions.
- Volume III entitled "*APIDRAIN Version 1.0, Process Drain Emission Calculator*" (API Publication Number 4681) is the computer model with user's guide to estimate emissions from refinery process drains. The software allows users to calculate VOC emissions based on the emission factors in Volume I and equations for speciated emissions in Volume II.

All three volumes of this study can be purchased separately; however, it is suggested that the user consider purchase of the entire set to gain a complete understanding of fugitive emissions from refinery process drains.

## TABLE OF CONTENTS

	<u>Page</u>
<b>EXECUTIVE SUMMARY</b>	
STATEMENT OF NEED.....	ES-1
IMPROVED MODEL.....	ES-1
CONCLUSIONS.....	ES-2
<b>1. INTRODUCTION</b>	
STATEMENT OF NEED.....	1-1
OBJECTIVES.....	1-1
SCOPE.....	1-2
ORGANIZATION OF REPORT.....	1-3
<b>2. TWO-ZONE EMISSIONS MODEL</b>	
MODEL OVERVIEW.....	2-1
Mass Transfer Fundamentals.....	2-1
Overview of Two-Zone Model.....	2-3
ZONE 1 SUBMODEL.....	2-4
ZONE 2 SUBMODEL.....	2-6
THE INTEGRATED MODEL.....	2-8
<b>3. EXPERIMENTAL METHODOLOGY</b>	
EXPERIMENTAL SYSTEMS.....	3-1
Laboratory Drain System (LDS).....	3-1
Trap Simulators.....	3-4
CHEMICAL TRACERS / TRACER PREPARATION.....	3-7
ANALYTICAL METHODS.....	3-9
Liquid Samples.....	3-9
Gas Samples.....	3-10
DATA ANALYSIS: OVERVIEW.....	3-11
Stripping Efficiencies.....	3-11
Mass Transfer Coefficients.....	3-11
ZONE 2 ANALYSIS.....	3-12
Experimental System (zone 2).....	3-12
Experimental Plan and Methodology (zone 2).....	3-14
Data Analysis (zone 2).....	3-19
ZONE 1 ANALYSIS.....	3-24
Experimental System (zone 1).....	3-24
Experimental Plan and Methodology (zone 1).....	3-25
Data Analysis (zone 1).....	3-28
QUALITY ASSURANCE.....	3-30
<b>4. EXPERIMENTAL RESULTS</b>	
ZONE 1.....	4-1
Experimental Results: Stripping Efficiencies.....	4-1
Correlations: Mass Transfer Parameters for Zone 1.....	4-5
ZONE 2.....	4-12
Experimental Results: Stripping Efficiencies.....	4-12
Correlations: Mass Transfer Parameters.....	4-15

**TABLE OF CONTENTS**

	<u>Page</u>
<b>5. MODEL INTEGRATION AND APPLICATIONS</b>	
SUMMARY OF EMISSIONS MODEL.....	5-1
Comparison With Existing Models .....	5-4
<b>6. SUMMARY AND CONCLUSIONS</b>	
SUMMARY.....	6-1
CONCLUSIONS.....	6-1
<b>7. REFERENCES .....</b>	<b>7-1</b>

**LIST OF TABLES**

	<u>Page</u>
Table 3-1. Volatile Tracers.....	3-7
Table 3-2. Summary of Tracer Bag Preparation .....	3-8
Table 3-3. Summary of Zone 2 Experiments.....	3-14
Table 3-4. Initial Liquid-Phase Tracer Concentrations in the Reservoir.....	3-15
Table 3-5. Liquid Sampling Schedule .....	3-16
Table 3-6. Gas Sampling Schedule For Zone 2 Experiments .....	3-18
Table 3-7. Summary of Air Entrainment Experiments .....	3-25
Table 3-8. Summary of Bubble Mass Transfer Experiments.....	3-26
Table 3-9. Summary of Surface Volatilization Experiments.....	3-27
Table 3-10. Analytical Liquid Standards Prepared from Tedlar™ Bag #7 .....	3-31
Table 3-11. Concentrations of Scott Specialty Gases Standards Cylinder.....	3-31
Table 3-12. Analytical Gas Standards Prepared from Scott Specialty Gases Cylinder.....	3-32
Table 3-13. Liquid- and Gas-Phase Method Detection Limits (MDLs) .....	3-33
Table 3-14. Mass Closure Analysis .....	3-36
Table 4-1. Stripping Efficiencies Due to Entrained Air Bubbles ( $\eta_b$ ) .....	4-3
Table 4-2. Zone 1 Stripping Efficiencies ( $\eta_1$ ).....	4-3
Table 4-3. Stripping Efficiencies Due to Surface Volatilization in a Trap ( $\eta_s$ ).....	4-4
Table 4-4. Measured Degrees of Equilibrium ( $\gamma$ ) for Entrained Bubbles .....	4-10
Table 4-5. Calculated Values of $K_L A_S$ .....	4-11
Table 4-6. Measured Stripping Efficiencies for Channel ( $\eta_2$ ).....	4-14
Table 4-7. Calculated Values of $K_L A_C$ .....	4-15
Table 4-8. Measured $k_g/k_l$ Ratios for the Underlying Sewer Channel (zone 2) .....	4-17
Table 5-1. Summary of Model Equations for Open Drains .....	5-1
Table 5-2. Summary of Model Equations for Trapped Drains (with water seals) .....	5-2
Table 5-3. Description of Variables .....	5-3

**TABLE OF CONTENTS**

**LIST OF FIGURES**

	<u>Page</u>
Figure 2-1. Different Emission Zones in an Industrial Process Drain.....	2-4
Figure 3-1. Schematic of Laboratory Drain System (LDS).....	3-2
Figure 3-2. Wind Tunnel in Place Over the Drain Hub .....	3-4
Figure 3-3. Schematic of Trap Simulator.....	3-5
Figure 3-4. J-Trap Arrangement Used During Zone 2 Experiments C9, C10, and C11 .....	3-13
Figure 3-5. LDS Configuration During Experiments C10 and C11.....	3-13
Figure 3-6. Gas Sampling Train.....	3-17
Figure 3-7. $K_{LA_c}$ Matrix Used to Determine $k_g/k_l$ Ratios.....	3-23
Figure 3-8. Estimating the Mass of Gas-Phase Tracer Leaving the LDS.....	3-35
Figure 4-1. Air Entrainment Rates Measured with Disintegrated Liquid Flows .....	4-6
Figure 4-2. Air Entrainment Rates Measured with Intact Liquid Flows.....	4-6
Figure 4-3. Toluene Stripping Efficiency for Experiment C5 .....	4-12
Figure 5-1. Integrated Model Compared with USEPA WATER8 Model (1994) (trapped drain, varying $Q_i$ ) .....	5-4
Figure 5-2. Integrated Model Compared with USEPA WATER8 Model (1994) (trapped drain, varying $H_c$ ) .....	5-5
Figure 5-3. Integrated Model Compared with BACT/LAER (open drain, varying $Q_i$ ).....	5-6
Figure 5-4. Integrated Model Compared with BACT/LAER (open drain, varying $H_c$ ) .....	5-7
Figure 5-5. Toluene Stripping Efficiency Versus Drain Ingassing Rate for an Open Drain...	5-8

## EXECUTIVE SUMMARY

### STATEMENT OF NEED

Industry continues to face increasingly stringent regulations related to volatile organic compound (VOC) emissions to the ambient atmosphere. Such emissions cause concern since most VOCs are photochemically reactive and contribute to the formation of ground level ozone in urban airsheds. Furthermore, many VOCs are also classified as hazardous air pollutants (HAPs) that pose risks to workers or the general public. These concerns cause a need for improved estimates of VOC and HAP emissions for many industrial sources, including process drains that serve as the initial point of wastewater collection in on-site industrial sewers. However, the number of process drains in a petroleum refinery can be in the thousands, making direct emission measurements costly and generally impractical. As such, emission factors and predictive models have been developed to estimate such emissions. Many of these factors and models are outdated or employ conservative assumptions that lead to significant overestimates of VOC emissions. There is a clear need for improved models to estimate VOC and HAP emissions from refinery process drains.

### IMPROVED MODEL

A two-zone emissions model was developed for estimating VOC emissions from refinery process drains. The model includes estimates of emissions from a water seal (zone 1) and an underlying channel (zone 2). For zone 1, the model includes estimates of air entrainment, degree of chemical equilibrium between entrained air bubbles and surrounding liquid, and gas- and liquid-phase mass transfer coefficients associated with volatilization across the upstream surface of a water seal. For zone 2, the model includes estimates of gas- and liquid-phase mass transfer coefficients in the channel below an active process drain.

Five volatile tracers and two separate experimental drains systems were used to develop model parameters. A total of 76 experiments were completed with the two experimental systems.

The two-zone model, including a description of all relevant variables and units, is presented in Chapter 5 of this report.

## CONCLUSIONS

Specific conclusions that resulted from this study are listed below:

1. Stripping efficiencies in water seals increase with increasing Henry's law constant and may approach 20% at moderate liquid temperatures (20 °C to 30 °C) for chemicals with Henry's law constants similar to or greater than toluene. However, stripping efficiencies for lower-volatility chemicals, e.g., acetone and ethyl acetate, should generally be on the order of 1% or lower.
2. Both air entrainment and surface volatilization are important contributors to mass transfer at water seals. For this study, the effects of surface volatilization were generally greater than those associated with entrained air.
3. Stripping efficiencies in water seals decrease substantially as the jet that impinges on the seal moves from a disintegrated film to a solid (intact) film. This is generally due to the effects of similar air entrainment rates but longer hydraulic residence times for the lower flows associated with disintegrated films.
4. Wind speed above a drain hub affects VOC emissions from drains with disintegrated process flows. However, the effects of wind on intact process flows appear to be small. The specific mechanism by which wind affects emissions during disintegrated flow conditions was not determined but could include increases in mass transfer coefficients, increases in interfacial area due to distortion of the falling film, increased ventilation of the drain throat, or some combination of the above.
5. Air entrainment rates in a water seal are significantly influenced by, and increase with, increases in process flowrate. Entrainment rates do not appear to be significantly influenced by the diameter of a drain throat or corresponding water seal.
6. The degree of chemical equilibrium between entrained air bubbles and surrounding liquid is highly dependent on Henry's law constant, and is also affected by changes in air entrainment rate. The degree of equilibrium increases with decreases in Henry's law constant and entrainment rate. It is reasonable to assume that chemicals with Henry's law constants as low as ethyl acetate and acetone will have a degree of equilibrium that approaches unity. However, highly volatile chemicals, e.g., cyclohexane or 1,3-butadiene, should have degrees of equilibrium that are generally less than 0.1 (10% of equilibrium). For these chemicals, an assumption of equilibrium for bubbles can lead to significant overestimation of emissions.

7. Stripping efficiencies associated with open drains are generally, but not always, greater than those for water seals for similar operating conditions. For this study, stripping efficiencies as high as 45% (cyclohexane) were observed for open drains.
8. Significant variations in stripping efficiency can occur as the operating conditions of open drains are varied. As with water seals, stripping efficiencies for open drains decrease as the process flowrate moves from being a disintegrated to a solid jet.
9. Elevated liquid temperatures can lead to substantial increases in chemical stripping efficiencies, particularly for lower-volatility chemicals. Increases in liquid temperature lead to increases in Henry's law constant, increases in mass transfer coefficients, and increases in buoyancy-induced ventilation.
10. The integrated two-zone model developed for this study should be a valuable tool for estimating VOC emissions from process drains. It is more mechanistic in nature than existing emissions models for process drains, and allows for an investigation of the effects of system operating conditions and chemical properties on VOC emissions.
11. An existing USEPA model (WATER8) may significantly overestimate stripping efficiencies, and subsequently emissions, from process drains that contain water seals.
12. Except in the case of highly-volatile chemicals, e.g., cyclohexane, BACT/LAER may underestimate VOC emissions and does not account for the mechanistic behavior of emissions as process operating conditions are varied.

# 1. INTRODUCTION

## STATEMENT OF NEED

Industry continues to face increasingly stringent regulations related to volatile organic compound (VOC) emissions to the ambient atmosphere. Such emissions cause concern since most VOCs are photochemically reactive and contribute to the formation of ground level ozone in urban airsheds. Furthermore, many VOCs are also classified as hazardous air pollutants (HAPs) that pose risks to workers or the general public. Emissions of such compounds are, or will soon be, regulated by industry-specific National Emission Standards for Hazardous Air Pollutants (NESHAPs).

The concerns listed above pose the need for improved estimates of VOC and HAP emissions for many industrial sources, including process drains that serve as the initial point of wastewater collection in on-site industrial sewers. However, the number of process drains in a petroleum refinery can number in the thousands, making direct emission measurements costly and generally impractical. Emission factors and predictive models have been developed to estimate such emissions. These factors and models are generally outdated, e.g., emission factors based on studies completed in the 1970s, or employ conservative assumptions, e.g., chemical equilibrium, that may lead to significant overestimates of VOC emissions.

There is a clear need for improved models to estimate VOC and HAP emissions from refinery process drains. A model based on fundamental mass transfer principles with mechanistic expressions that relate mass transfer parameters to system conditions should allow improved estimates of VOC and HAP emissions from process drains. Furthermore, such a model could be used to determine the effects of changes in system operating conditions and passive control strategies, e.g., inclusion of water seals and their effects on VOC emissions.

## OBJECTIVES

Specific objectives of this study are listed below:

1. Develop a state-of-the-art model to estimate VOC and HAP emissions from refinery process drains.

2. Determine model parameters based on a series of controlled experiments in laboratory-based drain simulators.
3. Develop empirical or semi-empirical relationships between model parameters and system operating conditions, environmental conditions, and chemical properties.
4. Use the experimental results and model to ascertain the relative significance of mass transfer mechanisms in process drains.
5. Compare the model developed for this study with those that have been used to estimate speciated VOC emissions from process drains.

## SCOPE

It was originally intended that a three-zone emissions model be developed with the ability to estimate VOC emissions from a falling film, water seal, and channel located below a drain. It was impossible to separate (experimentally) the effects of a falling film from volatilization in an underlying channel or water seal. As such, the effects of a falling film were "lumped" into mass transfer in an underlying channel or water seal.

Five volatile tracers were used in determining mass transfer parameters for the two-zone model. These tracers spanned a wide range of Henry's law constants, i.e.,  $0.0015 \text{ m}^3_{\text{liq}}/\text{m}^3_{\text{gas}}$  to  $7.3 \text{ m}^3_{\text{liq}}/\text{m}^3_{\text{gas}}$  at  $25 \text{ }^\circ\text{C}$ .

A total of 76 experiments were completed with the use of two separate experimental systems. Twelve of these experiments were completed to study gas-liquid mass transfer in the channel below a process drain. Forty experiments were completed to determine rates of air entrainment in a water seal. Seventeen experiments were completed to study the degree of chemical equilibrium between entrained air bubbles and surrounding liquid in a water seal. Seven experiments were completed to study volatilization across the upstream surface of a water seal. Four additional experiments were completed to ascertain volatilization from a falling film, but were inconclusive and not reported herein. No experiments were completed to determine emissions from a water seal below an inactive drain. No experiments were completed to assess gas-liquid mass transfer in the channel below inactive drains.

Several variables can affect mass transfer in a process drain. The primary variables that were studied included process flowrate, hydrodynamic regime (disintegrated or intact liquid

flow), and Henry's law constant. The effects of molecular-diffusion coefficients were accounted for in some correlations. The effects of temperature were accounted for through variations in liquid molecular diffusion coefficients, water viscosity and, most importantly, Henry's law constant.

## ORGANIZATION OF REPORT

The two-zone emissions model is described in Chapter 2. Chapter 3 includes a detailed description of experimental methods, including the two experimental systems that were employed, sample analysis procedures, and data analysis methods. Experimental results are presented in Chapter 4. The resulting two-zone model and parameter correlations are presented in Chapter 5. Several examples are provided to compare the model developed for this study with existing models for VOC emissions from process drains. An example is also provided to demonstrate the utility of the model for establishing whether water seals effectively reduce VOC emissions from process drains. A set of conclusions is provided in Chapter 6. References are provided in Chapter 7.

## 2. TWO-ZONE EMISSIONS MODEL

### MODEL OVERVIEW

A two-zone mechanistic emissions model is presented in this chapter. The model is intended to serve as a state-of-the-art tool for estimating chemical emissions from process drains. It is based on mass transfer kinetics, with parameters determined from a series of experiments described in Chapter 3. This chapter begins with a brief discussion of mass transfer fundamentals and terminology, as well as a conceptual description of the two-zone model. Mathematical expressions used to estimate gas-liquid mass transfer are then presented for each drain zone.

#### Mass Transfer Fundamentals

Equation 2-1, derived from a number of different mass transfer theories, can be used to calculate the mass flux across a gas-liquid interface (Lewis and Whitman, 1924; Higbie, 1935; Danckwerts, 1951; Dobbins, 1956):

$$r_a = K_L \left( C_l - \frac{C_g}{H_c} \right) \quad (2-1)$$

where:

$r_a$	=	flux across interface from liquid to gas (M/L <sup>2</sup> T)
$K_L$	=	overall mass transfer coefficient (L/T)
$C_l$	=	liquid-phase concentration of compound (M/L <sup>3</sup> )
$C_g$	=	gas-phase concentration of compound (M/L <sup>3</sup> )
$H_c$	=	Henry's law constant (L <sup>3</sup> <sub>liq</sub> /L <sup>3</sup> <sub>gas</sub> )

The term in brackets is often referred to as a concentration driving force, and represents how far a system is from a state of chemical equilibrium. The overall mass transfer coefficient,  $K_L$ , can be further reduced to its gas- and liquid-phase components. This concept, stemming from two-film theory, models mass transfer as a steady-state molecular diffusion process occurring

across two quiescent boundary films, one in the liquid phase and one in the gas phase (Lewis and Whitman, 1924):

$$\frac{1}{K_L} = \frac{1}{k_l} + \frac{1}{k_g H_c} \quad (2-2)$$

where:

- $k_l$  = liquid-phase mass transfer coefficient (L/T)
- $k_g$  = gas-phase mass transfer coefficient (L/T)
- $H_c$  = Henry's law constant ( $L^3_{liq}/L^3_{gas}$ )

The inverse of the overall mass transfer coefficient is often referred to as an overall resistance to mass transfer. This analogy to electrical resistance illustrates the liquid-phase ( $1/k_l$ ) and gas-phase resistance ( $1/k_g H_c$ ) to mass transfer.

Based on two-film (Lewis and Whitman, 1924), penetration (Higbie, 1935), and surface-renewal (Danckwerts, 1951) theories, the following relationships were developed. These relationships allow comparison of liquid- and gas-phase mass transfer coefficients for two different compounds:

$$\Psi_l = \frac{k_{li}}{k_{lj}} = \left( \frac{D_{li}}{D_{lj}} \right)^n \quad (2-3)$$

$$\Psi_g = \frac{k_{gi}}{k_{gj}} = \left( \frac{D_{gi}}{D_{gj}} \right)^m \quad (2-4)$$

where

- $\Psi_l, \Psi_g$  = mass transfer proportionality constants between compounds (-)
- $k_{li}$  = liquid-phase mass transfer coefficient for compound i (L/T)
- $k_{lj}$  = liquid-phase mass transfer coefficient for compound j (L/T)
- $k_{gi}$  = gas-phase mass transfer coefficient for compound i (L/T)
- $k_{gj}$  = gas-phase mass transfer coefficient for compound j (L/T)
- $D_{li}$  = liquid-phase molecular diffusion coefficient for compound i ( $L^2/T$ )

$D_{lj}$	=	liquid-phase molecular diffusion coefficient for compound j ( $L^2/T$ )
$D_{gi}$	=	gas-phase molecular diffusion coefficient for compound i ( $L^2/T$ )
$D_{gj}$	=	gas-phase molecular diffusion coefficient for compound j ( $L^2/T$ )
$n, m$	=	power constants (-)

The power constants  $n$  and  $m$  can vary from anywhere between unity (for two-film theory) and 0.5 (for penetration and surface-renewal theories). When a compound possesses an extremely large Henry's law constant, it may be possible to neglect the gas-phase resistance to transfer and thereby simplify Equation 2-2 to  $K_L \approx k_g$ . This is often done for oxygen, a commonly studied compound with an  $H_c$  value of  $32 \text{ m}^3_{\text{liq}}/\text{m}^3_{\text{gas}}$  at  $25^\circ\text{C}$ . Conversely, for very low volatility chemicals such as acetone, it is often possible to neglect the liquid-phase resistance altogether, and to express Equation 2-2 as  $K_L \approx k_g H_c$ . Once reference chemicals such as oxygen and acetone have been used to estimate liquid- and gas-phase mass transfer coefficients, Equations 2-3 and 2-4 can be used to calculate mass transfer coefficients for any compound.

### Overview of Two-Zone Model

Within a specific process drain, there are several locations where mass transfer can occur. In each case, different emission mechanisms are responsible. Figure 2-1 shows two typical process drains, one open and one trapped. Each drain is subdivided into one or two zones from which emissions may occur. Zone 1 extends from the bottom of the discharge nozzle to the water seal (inclusive of the water seal); mass transfer in this region is attributed to surface volatilization and air entrainment. The original intent of this study was to separate surface volatilization associated with the falling film from that associated with the underlying water seal. This proved to be experimentally difficult and, as such, the two surface volatilization components were "lumped" for zone 1. Based on the degree of splashing and the longer residence time within the water seal, i.e., relative to the falling film, it can be reasonably assumed that volatilization at the water seal is significantly greater than from the falling film.

Zone 2, present in both trapped and untrapped drains, follows the falling film as it impacts the underlying channel. In this zone, splashing in the channel is likely the primary emission mechanism.

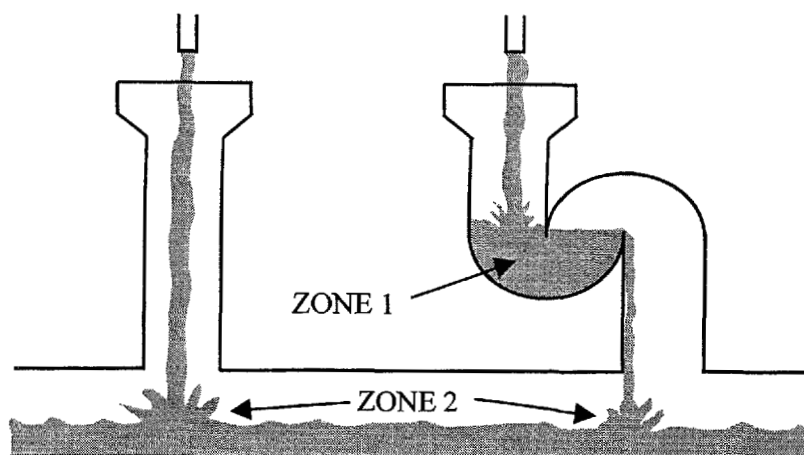


**Figure 2-1.** Different Emission Zones in an Industrial Process Drain

## ZONE 1 SUBMODEL

According to the American Petroleum Institute (API), over 80% of all petroleum refinery process drains are equipped with a water seal, provided by a P-trap, J-trap or similar device (American Petroleum Institute, 1996). As stated earlier, these water seals are designed to minimize the amount of fresh air entering the sewer, thus lowering the concentration driving force in the channel headspace and reducing VOC emissions. Even so, emissions still occur in a trapped drain. Zone 1 encompasses the falling film as well as the water seal (trap).

Within zone 1, it is assumed there are two major mechanisms by which chemicals can volatilize. The first involves surface volatilization which occurs from the falling film and the upstream surface of the water seal. Splashing is the most visible manifestation of this mechanism.

The second major mechanism is air entrainment induced by the boundary layer of air that surrounds the falling film as it descends into the drain. Small undulations along the surface of the film tend to "pull" air along in "pockets." When the falling film strikes the water below, these trapped air pockets are pulled below the water surface (Van de Sande and Smith, 1973). These air parcels break apart into many small air bubbles below the water surface, then return to the surface of the water seal. In larger traps, the bubbles return to the surface of the water seal, where they immediately outgas to the overlying drain throat. In smaller traps, the bubble

rise is often impeded by the impact of the falling film, causing the bubbles to recirculate within the water seal. It is assumed, based on repeated observations, that a negligible fraction of the entrained bubbles actually pass through the entire trap, i.e., most of them move within the upstream portion of the water seal and rupture upon resurfacing on the upstream side.

Several important assumptions were made in the development of the zone 1 model. First, the water seal itself was modeled as a continuous-flow stirred tank reactor (CFSTR). At the beginning of this study, dye (food coloring) was added to water that was pumped into the trapped drain. The dye was visually observed to almost immediately tint the water within the trap, confirming the CFSTR assumption.

Another assumption was that the gas-phase concentration within the drain throat is negligible. The gas boundary layer accompanying the falling film was presumed to ventilate the drain throat, preventing any gas-phase VOC accumulation. This assumption may be valid for high-volatility (high  $H_c$ ) VOCs, e.g., 1,3-butadiene, but may be violated for low-volatility chemicals, e.g., methanol. However, it was beyond the scope of this study to consider the drain throat as a separate zone.

Finally, it was assumed that all of the mass transfer in a water seal occurs along the upstream liquid-gas interface. Most water seals do have a downstream surface. However, observations have shown it to be very quiescent under most flow conditions, especially when compared to the upstream surface. Additionally, most water seals are installed to facilitate an approach to chemical equilibrium within the underlying channel. With these assumptions, the following expression can be used to represent total stripping efficiency for a water seal:

$$\eta_1 = 1 - \frac{1}{1 + \frac{Q_e}{Q_l} H_c \gamma + \frac{K_L A_s}{Q_l}} \quad (2-5)$$

where:

- $\eta_1$  = fractional stripping efficiency for zone 1 (-)
- $K_L A_s$  = mass transfer coefficient for surface volatilization ( $L^3/T$ )
- $Q_e$  = air entrainment rate ( $L^3/T$ )

- $Q_i$  = process flowrate into drain ( $L^3/T$ )  
 $\gamma$  = extent of chemical equilibrium in the entrained bubbles (-)  
 $H_c$  = Henry's law constant ( $L^3_{liq}/L^3_{gas}$ )

The  $\gamma$  term should vary between 0 and 1. A value of  $\gamma = 1.0$  corresponds to a condition of chemical equilibrium between gas within the bubble and the surrounding liquid. It is assumed that air that is initially entrained below the water surface is devoid of VOCs.

The mass transfer coefficients and interfacial areas are lumped together and expressed as " $K_L A$ " values in Equation 2-5. From this point forward, the term "mass transfer coefficient" will refer to both  $K_L$  and  $K_L A$  terms interchangeably.

In zone 1, there are a total of four parameters that must be determined empirically: the liquid and gas-phase mass transfer coefficients for surface volatilization ( $k_l A_s$ ,  $k_g A_s$ ), the degree of equilibrium term ( $\gamma$ ), and the volumetric flowrate at which air is entrained into the water seal ( $Q_e$ ).

Air entrainment as a result of a liquid jet impacting upon a liquid surface has been the subject of several experimental investigations. These studies used high speed pressurized water jets (Bin, 1993 and Van de Sande, 1976), and are thus not applicable for estimation of air entrainment in typical trapped process drains.

## ZONE 2 SUBMODEL

Zone 2 accounts for mass transfer which occurs when the process flow enters the sewer reach. Emissions in zone 2 are primarily due to splashing which occurs when the process flow impacts any liquid that might be in the channel or the channel bottom itself. Mass transfer due to air entrainment may also occur in the channel, but only when a sufficient depth of water exists in the sewer reach. For the purpose of the zone 2 model, both the gas and liquid phases were treated as CFSTRs. Simultaneous steady-state mass balances on gas and liquid phases can be used to derive an expression for zone 2 emissions.

Due to shear forces associated with the descending liquid film, it is assumed that an active open drain will always ingas. Once this air has entered the sewer, it will combine with whatever air is flowing down the sewer reach and will continue traveling in the same direction as the channel ventilation. It is further assumed that there is negligible gas-phase VOC entering zone 2 via the drain throat. In a trapped drain, the gas flowrate in the drain throat was assumed to be zero, while in an open drain it was assumed that the gas-phase concentration in the drain throat is negligible, as with zone 1. These assumptions result in the following expressions for stripping efficiency:

$$\eta_2 = 1 - \frac{(Q_1 + Q_c) \left( \frac{Q_c C_{co} + Q_1 C_{lo} + \frac{K_L A_c Q_{gc} C_{gc}}{H_c Q_{gc} + H_c Q_{gd} + K_L A_c}}{Q_c + Q_1 + K_L A_c - \frac{(K_L A_c)^2}{H_c Q_{gc} + H_c Q_{gd} + K_L A_c}} \right)}{Q_c C_{co} + Q_1 C_{lo}} \quad (2-6)$$

where:

- $\eta_2$  = fractional stripping efficiency for zone 2 (-)
- $Q_1$  = process flowrate into drain ( $L^3/T$ )
- $Q_c$  = upstream liquid channel flowrate ( $L^3/T$ )
- $C_{lo}$  = liquid-phase concentration entering the zone ( $M/L^3$ )
- $C_{co}$  = upstream liquid channel concentration ( $M/L^3$ )
- $K_L A_c$  = mass transfer coefficient for channel effects ( $L^3/T$ )
- $C_g$  = gas-phase concentration in channel headspace ( $M/L^3$ )
- $Q_{gc}$  = upstream headspace gas flowrate ( $L^3/T$ )
- $C_{gc}$  = upstream headspace gas concentration ( $M/L^3$ )
- $Q_{gd}$  = gas flowrate drawn down process drain throat ( $L^3/T$ )
- $C_{gd}$  = gas concentration of gas drawn down process drain throat ( $M/L^3$ )
- $H_c$  = Henry's law constant ( $L^3_{liq}/L^3_{gas}$ )

Only in zone 2 does the stripping efficiency include channel flow as well as process flow. Aqueous phase chemicals, entering the region of the drain from some point upstream, may volatilize as they pass through the channel splash zone. There are several possible factors contributing to emissions from zone 2. As with zone 1, liquid velocity may be an important factor. Emission rates may also be a function of whether or not the process flow is aligned with the drain throat. When the flow is misaligned, it strikes the drain hub and adheres to the walls of the throat as it descends into the sewer reach. A similar effect is observed when a J-trap is in place above the channel. The extent of air flow into the mass transfer zone should have an effect on gaseous accumulation, and thus mass transfer, but may also affect gas-phase resistance to mass transfer.

## THE INTEGRATED MODEL

By sequentially applying the stripping efficiencies for zones 1 and 2, the total fractional stripping efficiency associated with a process drain can be estimated. The stripping that occurs in one emission zone is accounted for when calculating stripping effects from the downstream zone:

$$\eta_d = \eta_1 + \eta_2(1 - \eta_1) \quad (2-7)$$

where:

- $\eta_d$  = total stripping efficiency for process drain (-)
- $\eta_1$  = stripping efficiency for zone 1 (-)
- $\eta_2$  = stripping efficiency for zone 2 (-)

In situations where there are fewer than two active emission zones, Equation 2-7 is still valid, providing that the stripping efficiency term for the missing emission zone is set to zero. This would be the case for an open drain, or even a trapped drain, if the user was confident that a state of chemical equilibrium existed in the underlying channel. Calculating the total stripping efficiency is complicated somewhat by the possible presence of chemicals flowing into zone 2 from upstream drains. Equation 2-7 becomes inapplicable under such conditions; it can only be

used to calculate the stripping from one waste stream. For the more complex scenario of mass flow from upstream drains, the following expressions should be used:

$$\eta_d = 1 - \frac{(1 - \eta_2)(Q_c C_{co} + Q_1 C_{lo} [1 - \eta_1])}{Q_c C_{co} + Q_1 C_{lo}} \quad (2-8)$$

where:

- $\eta_d$  = total stripping efficiency (process drain with channel flow) (-)
- $\eta_1$  = stripping efficiency for zone 1 (-)
- $\eta_2$  = stripping efficiency for zone 2 (-)
- $Q_c$  = upstream liquid channel flowrate (L<sup>3</sup>/T)
- $Q_1$  = process flowrate into drain (L<sup>3</sup>/T)
- $C_{lo}$  = liquid-phase concentration in process discharge to drain (M/L<sup>3</sup>)
- $C_{co}$  = upstream liquid channel concentration (M/L<sup>3</sup>)

If either  $Q_c$  or  $C_{co}$  is zero, Equation 2-8 reverts to the simpler Equation 2-7. Once the fractional stripping efficiency has been determined, the gaseous emission rate from a process drain is easily calculated. It is simply equal to the total stripping efficiency multiplied by the mass rate at which a VOC enters the drain in the liquid phase:

$$E = \eta_d (Q_c C_{co} + Q_1 C_{lo}) \quad (2-9)$$

where:

- $E$  = process drain emission rate (M/T)
- $\eta_d$  = total stripping efficiency for process drain (-)
- $Q_c$  = upstream liquid channel flowrate (L<sup>3</sup>/T)
- $Q_1$  = process flowrate into drain (L<sup>3</sup>/T)
- $C_{lo}$  = liquid-phase concentration in process discharge to drain (M/L<sup>3</sup>)
- $C_{co}$  = upstream liquid channel concentration (M/L<sup>3</sup>)

### 3. EXPERIMENTAL METHODOLOGY

#### EXPERIMENTAL SYSTEMS

Two experimental systems were constructed in an environmental chamber at The University of Texas at Austin. A laboratory drain system (LDS) and three trap simulators were designed to isolate different VOC emission mechanisms and to allow the determination of important mass transfer parameters. Originally, all of the experiments except those investigating temperature effects were to be conducted at a temperature of 20 °C. However, during the course of the study, the climate control equipment in the environmental chamber housing the LDS and trap simulators failed. The remainder of the experiments were completed at liquid and air temperatures ranging between 21 and 25 °C.

##### Laboratory Drain System (LDS)

A pilot-scale process drain and sewer reach was constructed at The University of Texas at Austin. The system, as shown on Figure 3-1, consisted of a channel, a tracer reservoir, and accompanying pumps, piping, and miscellaneous equipment. It was similar to the system used previously by Shepherd (1996).

The channel was comprised of six or seven glass pieces: three reach sections, two end caps, a drain hub, and sometimes a J-trap, all of which were connected to one another by beaded glass couplings. The channel sections each had an inside diameter (i.d.) of 15 cm and a length of 46 cm. Two channel sections were fitted with 5 cm i.d. vertical risers, each extending 30.5 cm above the crown of the sewer channel. The upstream riser served as the active drain throat. During open drain experiments, a removable glass reducer (10 cm by 5 cm) was attached to this riser to help simulate an actual drain hub. During experiments where a water seal was desired, the hub shown on Figure 3-1 was removed and a 5 cm i.d. glass J-trap was fastened in its place. The reducer (hub) was then re-attached to the top of the J-trap to complete the drain arrangement. The downstream riser allowed for the outgassing of air drawn into the channel headspace by falling process flow. For experiments where channel ventilation was not desired, glass end caps were placed over the downstream riser.

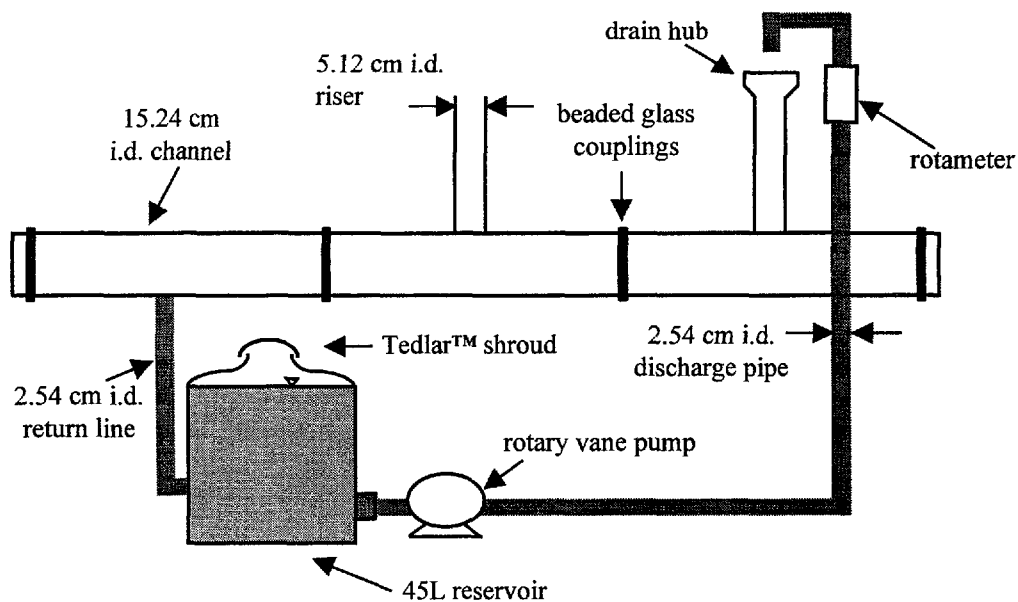


**Figure 3-1.** Schematic of Laboratory Drain System (LDS)

The final channel section had a 4 cm i.d. riser. This riser, which was further reduced to a 2.5 cm diameter, was pointed downwards, and served as the channel drain. A 4 cm<sup>2</sup> section of stainless steel mesh was placed at the inlet of the return pipe; its purpose was to prevent the formation of drain vortices, which were observed to occur when there was a high process flowrate and/or low water level in the channel. Both ends of the channel were sealed with a glass end cap. As volatilization from the quiescent water surface of the sewer channel was competing with drain emissions as a mass transfer mechanism, an effort was made to minimize its effect. To reduce the channel surface area across which volatilization could occur, the reach was made as short as possible. The total reach length was 1.5 meters.

The tracer reservoir was a 45 liter glass carboy, narrowed at the top to minimize the air-water interfacial area. During experiments, the top opening was covered with a sheet of inert Tedlar™, secured with duct tape. This minimized the amount of air exchange between the reservoir headspace and the ambient air. The entire reservoir was placed on top of cinder blocks and plywood spacers. By adding or removing spacers, the carboy could be raised or

lowered slightly, allowing complete control over the depth of water in the channel. Three ports were fitted to the reservoir. The return water from the channel entered the reservoir via one of these ports. Another port drew water into the process pump. The final port was a small Teflon™ stopcock inserted in a small hole in the side of the carboy and sealed with silicone. As described later, this stopcock was used for the collection of liquid samples.

A mixing motor (Cole Parmer, Stir Pak), supported by a stand, was used to rotate a stainless steel shaft and propeller that were inserted into the reservoir to mix the water. This mixing ensured that the behavior of the reservoir approached that of a CFSTR. To prevent vortexing, the shaft was tilted at a slight angle and closely controlled.

A variable speed rotary vane pump (PROCON, Model 7116-15) was used to convey water through the system. It drew water from the reservoir and pumped it up a 1.7 m stretch of 2.5 cm i.d. Teflon™ pipe equipped with an in-line rotameter (King, Model K72-05-0161), for flow measurements. Several Teflon™ elbows then redirected this flow so it was aligned with the drain hub.

A wind tunnel was used to simulate the effects of wind passing over a process drain (Figure 3-2). The tunnel was composed of wire mesh wrapped with plastic sheeting, and could be placed over the drain riser when necessary. A small fan (Tatung, Model LC-12) was used to force a flow of air over the drain riser. A rheostat was used to control the wind speed. A thermoanemometer (Alnor® model 8565) was used to determine wind speeds within the tunnel. Anemometer traverses completed immediately upstream of the drain hub indicated uniform velocity profiles for all wind speeds.

Whenever possible, inert materials such as Teflon™ and glass were selected for use in the experimental system. Threaded 2.5 cm i.d. Teflon™ pipes comprised the majority of the process conduits, i.e., leading from the reservoir to the process drain nozzle. However, in some locations where physical flexibility was required to ensure structural integrity, short (2 - 3 cm) sections of Tygon™ tubing were used. Examples of such locations included the process pump inlet and return pipe reservoir inlet. Both connections were subjected to some bending and flexing.

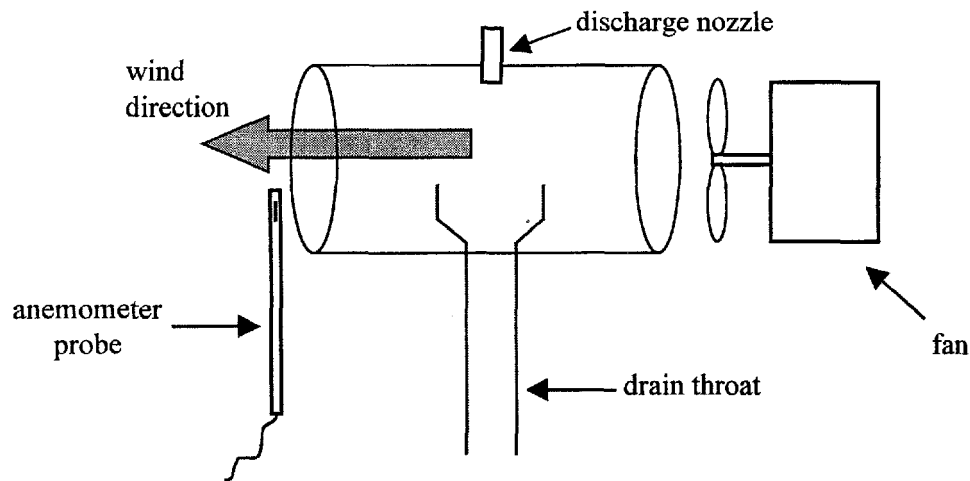


**Figure 3-2.** Wind Tunnel in Place Over the Drain Hub

The channel and reservoir were each composed of glass. The flow rotameter was comprised of an acrylic polymer casing and a stainless steel float. Stainless steel was also used in the pump impeller, the return pipe vortex suppresser, a pipe fitting, and the mixer shaft and propeller. Silicone caulk was used to seal the sampling and return ports on the reservoir. Previous research on an earlier version of the LDS indicated that incidental losses due to chemical sorption to solid surfaces were small relative to chemical stripping, and could be neglected (Shepherd, 1996). Nearly the same group of chemical tracers was used in each research effort.

### Trap Simulators

Three full-scale P-traps were purchased and modified for use in this research. These polyvinyl chloride (PVC) traps, referred to as trap simulators, were used to determine two important operating parameters for zone 1: the degree of equilibrium of entrained air bubbles ( $\gamma$ ) and the volumetric rate at which air is entrained within the water seal ( $Q_e$ ). The three trap simulators had inside diameters of 5, 7.6, and 10 cm. An example of a trap simulator is illustrated on Figure 3-3.

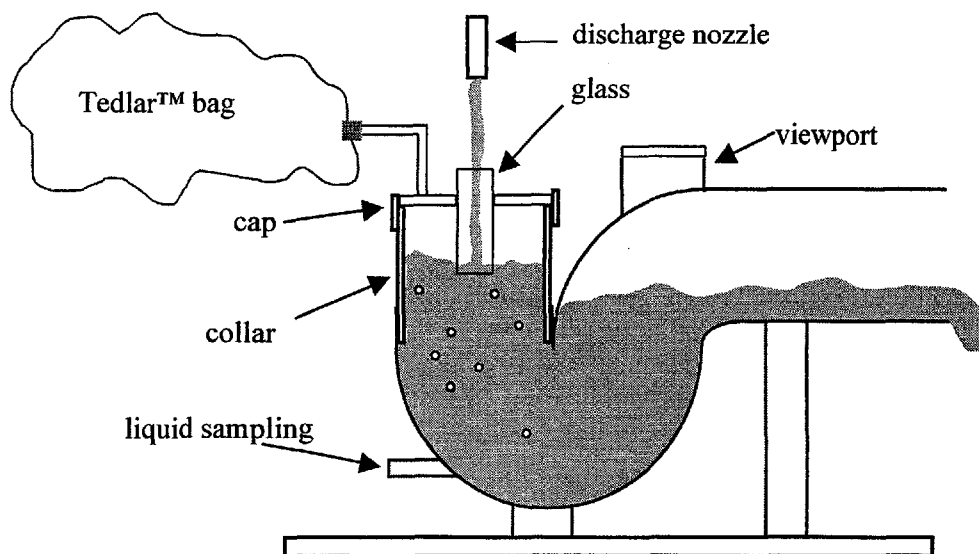


**Figure 3-3.** Schematic of Trap Simulator

The traps were mounted on small blocks of wood, which in turn were mounted on sections of water-resistant particle board. Steel straps held the traps in place and ensured that they were upright at all times. A small viewing port was attached to each trap simulator allowing for the determination of whether or not entrained air bubbles were passing through to the downstream surface of the water seal.

Water was drawn from the 45 L glass reservoir by means of a variable speed rotary vane pump (PROCON, Model 7116-15). Water was pumped through a section of Teflon™ pipe and rotameter before discharging into the trap. A mixing motor and propeller were used to assure a uniform tracer concentration in the reservoir. The water delivery arrangement was almost identical to that used for the LDS, but there were several important differences. The trap simulator was a “flow through” system; once water had passed through the pump and the trap, it would discharge into a laboratory sink. Each experiment lasted only as long as there was water in the reservoir, typically less than six minutes. However, this flow-through configuration allowed a steady-state condition to be reached within the J-trap as the influent liquid concentration was observed to remain constant over time.

When falling toward the water seal, the process flow would pass through a small glass cylinder inserted in a plexiglass cap and extending just below the surface of the water seal. As the falling film impacted the underlying water surface, air bubbles were entrained within the water seal. This cylinder served several important purposes. First, it was large enough to allow for the gaseous boundary layer that is dragged along a falling film to impinge upon the underlying trap, thus allowing for the entrainment of air bubbles. Secondly, it was small enough in diameter such that most of the entrained air bubbles would not rise back up into the impingement zone defined by the cylinder. Finally, the cylinder acted to suppress agitation (splashing) within the enclosed headspace thus suppressing the effects of surface volatilization, or conversely isolating the effects of mass transfer due to air entrainment. These bubbles then surfaced and ruptured within an enclosed headspace, confined by the water seal on one end and the cap on the other. This led to a pressurization of the headspace; to relieve this pressure, the gas was allowed to exit through a small relief port built into the plexiglass cap. The gas then flowed through a small section of 6 mm i.d. Teflon™ tubing and several Swagelok™ fittings before filling an attached Tedlar™ bag. Liquid samples were collected from a Teflon™ stopcock (liquid sampling port) inserted into the body of the trap.

For the purpose of the emissions model, both the water seal and enclosed headspace were assumed to behave as CFSTRs. Whenever possible, the volume of the enclosed headspace was minimized. Because these were flow-through experiments, samples could not be collected until a steady-state condition was achieved in both the water seal and the headspace. Reaching steady-state conditions usually required the throughput of two or three gas turnovers in the headspace. By minimizing the volume of the enclosed headspace, the time required to reach steady-state conditions was reduced. This was particularly important considering that each experiment lasted only a few minutes. However, there was a minimum bound to the headspace volume. If the volume was too small, plugs of water would be drawn into the gas sampling line, thus rendering the gas sample inaccurate. To closely control the headspace volume, a set of PVC collars were used. These collars, cut to length in 6 mm increments, were placed between the actual body of the trap and the plexiglass cap. Each trap simulator had its own set of collars, with an outside diameter equal to that of the trap's inside diameter.

When performing experiments with trap simulators, it was desirable to maximize the fraction of entrained air that was captured in the Tedlar™ bag. Bubbles that surfaced within the area of the glass cylinder may not have been captured. Therefore, an effort was made to minimize the required cross-sectional area of the glass cylinder. For each trap simulator, a set of three plexiglass caps and glass cylinders were fabricated. The glass cylinders had diameters of 1.9 cm, 2.5 cm, and 3.2 cm; openings in the caps were sized accordingly.

## CHEMICAL TRACERS / TRACER PREPARATION

Five compounds, covering a wide range of Henry's law constants, were selected as chemical tracers for use in mass transfer experiments. These were acetone, ethyl acetate, toluene, ethylbenzene, and cyclohexane. As seen by the Henry's law constants in Table 3-1, acetone and ethyl acetate were selected as low-volatility tracers, for which gas-phase resistance to mass transfer should be significant. Toluene and ethylbenzene represent moderately volatile chemicals; their mass transfer is affected by both gas- and liquid-phase resistances. Cyclohexane was chosen as a high volatility chemical, for which liquid-phase resistance should govern mass transfer.

**Table 3-1.** Volatile Tracers

Tracer	Henry's Law Constant, $H_c$ ( $m^3_{liq}/m^3_{gas}$ ) at 25 °C
Acetone	0.0015
Ethyl acetate	0.0049
Toluene	0.27
Ethylbenzene	0.33
Cyclohexane	7.32

The  $H_c$  values presented in Table 3-1 are valid only at 25 °C. During the course of this research, recorded liquid temperatures ranged between 19.7 and 33.1 °C. Since  $H_c$  is a strong function of temperature, it was necessary to find relationships between  $H_c$  and temperature. For toluene, ethylbenzene, and cyclohexane,  $H_c$  - temperature correlations were developed by Ashworth *et al.* (1988) and employed in this study. However, for acetone and ethyl acetate, no such correlations existed. To develop correlations for these tracers, it was first assumed that their solubility was relatively insensitive to temperature changes within the range tested. Then,

by knowing the  $H_c$  value at 25 °C, it was possible to express the Henry's law constant as a function of the chemical's vapor pressure, as shown in Equation 3-1:

$$H_c = H_c(25^\circ\text{C}) \frac{P^\circ(T_{\text{liq}})}{P^\circ(25^\circ\text{C})} \quad (3-1)$$

where:

$P^\circ$  = chemical's vapor pressure (atm)  
 $T_{\text{liq}}$  = liquid temperature (°C)

Besides their ranges in volatility, there were other criteria considered when selecting chemical tracers. Safety and ease of handling was one, i.e., toluene was chosen over benzene. Choosing chemicals with varying boiling points was also important to ensure effective chromatographic peak resolution.

One day before each set of experiments, tracer solutions were prepared using 3 liter Tedlar™ bags. Between 1 and 4 mass transfer experiments could be completed on any one day. For every experiment, three Tedlar™ bags were filled with tap water and spiked with chemical tracers according to the amounts listed in Table 3-2. For each set of experiments, a common bag for making liquid standards (#7) was also prepared.

**Table 3-2. Summary of Tracer Bag Preparation**

Bag #	Water Volume (liters)	Acetone (mL)	Ethyl Acetate (mL)	Toluene (mL)	Ethylbenzene (mL)	Cyclohexane (mL)
1	2	2	1.4	0	0.3	0.13
2	2	2	0	0.5	0.3	0.13
3	2	2	1.4	0.4	0.3	0.13
7 (stds)	0.75	0.75	0.35	0.09	0.09	0.052

The injection pattern was chosen to ensure that syringe injections were evenly distributed over all of the bags. Even so, the septa of the Tedlar™ bags were replaced after every fifty piercings, or whenever leakage or visible deterioration was observed.

Tracer bags were prepared in the following fashion. The required volume of deionized water was first measured in a graduated cylinder and then poured into a glass beaker. A peristaltic pump (Cole Parmer, Model 7553-70) was then used to transfer the water into the Tedlar™ bag. Gas-tight syringes (Hamilton) were used to inject desired volumes of pure chemical tracers into the bags. Before each set of injections, the syringe was flushed three times with methanol, three times with deionized water, and, finally, three times with the chemical which was to be injected next. By adding the tracer volumes specified in Table 3-2, the concentrations in each Tedlar™ bag were below the solubility limits of each tracer. After all the chemicals were added, the Tedlar™ bags were agitated for two minutes by repeated pressure on each bag. The mixtures were then left overnight under a fumehood. This helped ensure that by the time of the experiment the chemicals had completely dissolved into the water. Between each experiment, the Tedlar™ bags were each filled and drained three times with clean water to desorb.

## ANALYTICAL METHODS

### Liquid Samples

Liquid samples and standards were analyzed with a gas chromatograph (Hewlett Packard model 5890 Series II Plus) equipped with a flame ionization detector (FID). A 5 m HP-1 capillary column was installed in the GC (0.53 mm i.d., 2.65  $\mu\text{m}$  film thickness). Samples were prepared for analysis by a headspace concentrator equipped with an autosampler (Tekmar Model 7000).

Liquid samples were usually placed in the autosampler within 24 hours of their collection. During the period between collection and analysis, vials were stored in an environmental chamber maintained at 4 °C. Previous research has shown that vials stored in such a manner suffered minimal tracer losses, even after seven days of storage (Shepherd, 1996).

Once in the autosampler, vials were automatically placed into a 70 °C internal platen. Vials remained in this platen for a period of 60 minutes, during which time a state of chemical equilibrium was reached between the vials' liquid and headspace. The headspace of each vial was then pressurized with chromatographic grade helium for a period of 1 minute. A sample

loop, contained within the autosampler and maintained at 100 °C, was then filled with headspace gas and allowed to stabilize. After a period of 1.2 minutes, the autosampler injected this gas into the GC. The total injection time lasted 1 minute.

The GC inlet temperature was set at 200 °C and the detector temperature at 250 °C. The total GC run time was 2.65 minutes per liquid sample. For the first 30 seconds of each run, the GC oven was maintained at 32 °C. The temperature was then ramped upward at a rate of 20 °C/min, until a temperature of 55 °C was reached. This higher temperature was maintained for one minute, after which time the GC run was concluded. The GC was controlled by HP 3365 Chemstation Version A.03.34 software, operated from a personal computer. This same program was also used to store, retrieve, and interpret GC data.

### Gas Samples

Gas samples were analyzed within four days of being collected. Sorbent tubes were stored in a 4 °C environmental chamber between the time they were sampled and the time they were analyzed. As with liquid vials, previous research indicated that this manner of storage results in minimal sample deterioration, even after a week or more (Fitzgerald, 1996).

Gas samples and standards were analyzed with a gas chromatograph equipped with a flame ionization detector (FID) (Hewlett Packard model 6890). A 30 m capillary column was installed in the GC (Restek model 10908, 0.53 mm i.d., 3.00 µm film thickness). To analyze gas samples, sorbent tubes were first placed in a thermal desorber (Tekmar 1600 Aerotrap). Each tube was rapidly heated to 250 °C. For a period of 8 minutes, chromatographic grade helium was swept through the heated tube. Chemicals removed from the tube were concentrated on an internal Tenax™ trap located in a purge and trap controller (Tekmar 3000). The internal trap was then desorbed for two minutes at 250 °C and tracers were carried by helium gas to the GC injection port.

Both the inlet and detector temperatures were set at 250 °C. The total GC run time was 14.60 minutes per gas sample. For the first 30 seconds of each run, the GC oven was maintained at 34 °C. The temperature was then ramped upward, at a rate of 10 °C/min, until a temperature of 65 °C was reached. This temperature was then maintained for 11 minutes, after

which time the GC run would terminate. The GC was controlled by HP Chemstation Version A.04.02 software operated from a personal computer. This same program was also used to store, retrieve and interpret GC data. Following analysis, each sorbent tube was conditioned in a thermal conditioner (Tekmar Thermotrap). For a period of one hour, 300 °C chromatographic grade nitrogen was allowed to flow through each tube, removing residual tracers from the adsorbent. The conditioned tubes were then capped by stainless steel Swagelok™ end caps (with Teflon™ ferrules).

## DATA ANALYSIS: OVERVIEW

### Stripping Efficiencies

Following each mass transfer experiment, a fractional stripping efficiency was determined for each chemical tracer. As expressed by Equation 3-2, stripping efficiency was defined as the mass fraction of liquid-phase VOC that volatilized as the wastewater passed through a particular system or emissions zone:

$$\eta = 1 - \frac{Q_l C_{out}}{Q_l C_{in}} \quad (3-2)$$

where:

- $\eta$  = stripping efficiency (-)
- $C_{in}$  = liquid-phase VOC concentration entering the system (M/L<sup>3</sup>)
- $C_{out}$  = liquid-phase VOC concentration exiting the system (M/L<sup>3</sup>)
- $Q_l$  = liquid flowrate (L<sup>3</sup>/T)

In a recirculating batch system such as the LDS, if  $C_{in}$  represents the liquid concentration at any moment,  $C_{out}$  represents the new concentration after the passage of one hydraulic residence time.

### Mass Transfer Coefficients

This study was intended to quantify the following mass transfer parameters: fractional stripping efficiencies, air entrainment rates (where applicable), and overall mass transfer coefficients for two different emission zones at a variety of operating conditions. Overall mass transfer coefficients were then divided into individual gas- and liquid-phase components. These

$k_LA$  and  $k_gA$  values, along with air entrainment rates, were then subjected to a non-linear regression analysis. The goal of this analysis was to develop mathematical correlations for expressing these terms as functions of environmental and drain operating conditions. Once correlated, these terms were incorporated into the integrated emissions model.

## ZONE 2 ANALYSIS

Zone 2 is generally less complex than zone 1 in as much as it only involves one mass transfer parameter and one experimental system. As such, the zone 2 analysis is described first, followed by an analysis of zone 1 experiments.

The volatilization of VOCs can occur anywhere along the sewer channel. However, zone 2 represents the final area where turbulence associated with impinging process flow can directly lead to VOC emissions. A series of 12 mass transfer experiments were completed for this zone, encompassing a wide variety of operating conditions. The objective was to calculate stripping efficiencies and mass transfer coefficients.

### Experimental System (zone 2)

The LDS was used for all zone 2 experiments. During open drain experiments, the discharge nozzle was positioned approximately 1 centimeter above the top of the drain hub. The distance from the discharge nozzle to the channel invert was 70 cm.

During trapped drain experiments, a glass 5 cm i.d. J-trap was attached to the top of the drain riser. The discharge nozzle was then extended into the trap, so that the outlet was submerged under the water seal surface. This effectively eliminated the falling liquid film and entrained air bubbles. The nozzle was extended by connecting a Teflon™ pipe coupling to the nozzle outlet and then another 2.5 cm i.d. Teflon™ pipe to the other end of the coupling (Figure 3-4).

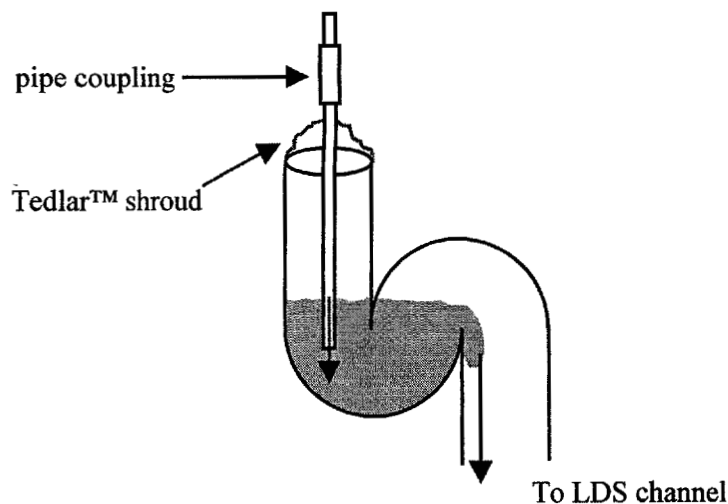


**Figure 3-4.** J-Trap Arrangement Used During Zone 2 Experiments C9, C10 and C11

A Tedlar™ shroud was draped over the drain throat and sealed using duct tape. This ensured minimal tracer losses from volatilization at the upstream surface of the water seal. During two trapped drain experiments, it was necessary to force-ventilate the channel to prevent gas-phase tracer accumulation in the headspace. This was accomplished by replacing the upstream channel end cap (Figure 3-5) with a similar end cap containing a 2.5 cm opening. An 8 mm i.d. Tygon™ tube was inserted into this opening. This hose was attached to a high pressure air spigot to force air through the channel headspace and out the downstream riser.

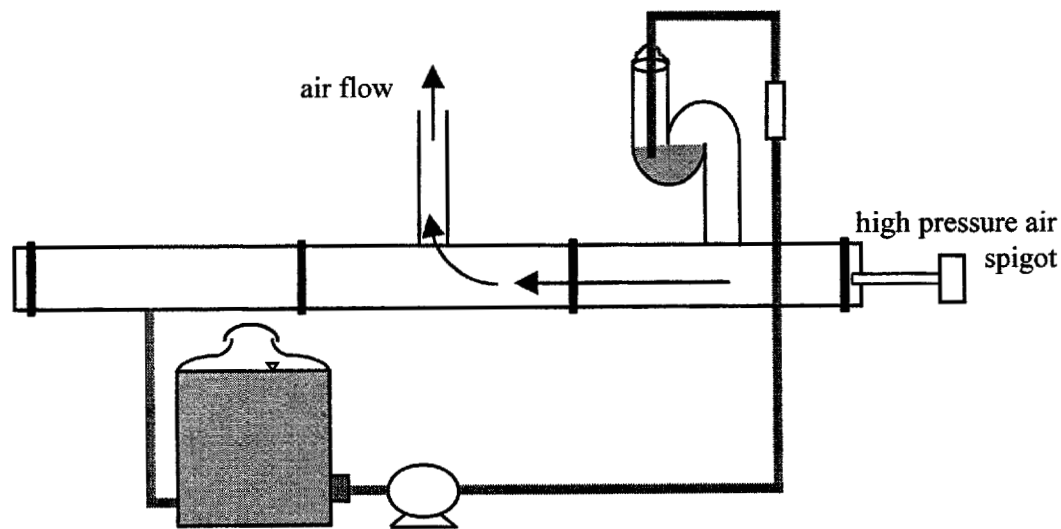


**Figure 3-5.** LDS Configuration During Experiments C10 and C11

### Experimental Plan and Methodology (zone 2)

The purpose of each zone 2 experiment was to calculate a fractional stripping efficiency and an overall mass transfer coefficient,  $K_L A_c$ . In the channel, it was suspected that both air entrainment and surface volatilization played significant roles in mass transfer. However, due to the difficulty in isolating these mechanisms, a “lumped” mass transfer coefficient was adopted. A summary of zone 2 experiments is presented in Table 3-3.

**Table 3-3.** Summary of Zone 2 Experiments

Expt. #	Liquid Flowrate (L/min)	$T_{liq}$ (°C)	Drain Configuration
C1	3.8	21.7	straight drain
C2	7.6	21.7	straight drain
C2-B	7.6	23.9	straight drain
C3	11.4	20.6	straight drain
C4	15.1	20.4	straight drain
C5	7.6	33.1	straight drain
C6	7.6	20.1	straight drain, misaligned hub
C7	15.1	21.8	straight drain, misaligned hub
C8	7.6	20.0	straight drain, empty channel
C9	7.6	19.7	trapped drain
C10	11.4	24.0	trapped drain, force ventilated headspace
C11	15.1	24.5	trapped drain, force ventilated headspace

Experiments C1 through C4 were intended to establish a relationship between the process flowrate and the overall mass transfer coefficient. During Experiment C5, the environmental chamber was heated in order to observe the effects of high temperature on mass transfer. Experiments C6 and C7 were completed to investigate the effects of a misaligned drain hub. This condition, common in industrial facilities, can result in significantly different patterns of splashing than those associated with a properly aligned process flow. During Experiment C8, the channel, which was usually maintained at approximately 20% full, was almost completely emptied. Experiments C9 through C11 were completed in order to study the mass transfer that occurs downstream of a water seal, as the process flow pours out of the water seal and into the sewer reach. During Experiments C10 and C11, the channel headspace was force-ventilated. The force ventilation was intended to prevent gas accumulation in the headspace. During several previous trapped experiments, a state of

chemical equilibrium had been reached so quickly in the channel headspace that it was impossible to derive meaningful mass transfer coefficients.

Before each experiment, the reservoir was filled with 40 L of tap water from a faucet within the environmental chamber. In some cases, when the observed water depth in the channel was below about 1.5 cm, an additional liter of water was added to the reservoir; a water depth between 1.5 and 2.5 cm was desirable. Usually, the tap water was approximately the same temperature as the air. However, during some experiments the water was significantly warmer or cooler than the surrounding air. In these cases, the reservoir was filled at least three hours before an experiment to allow the water to adjust to the temperature of the ambient air.

The final task before the beginning of an experiment was to introduce the tracer chemicals into the reservoir. Each of the three Tedlar™ tracer bags were brought into the environmental chamber and attached to a peristaltic pump (Cole Parmer, Model 7553-76). The contents of the bags were then pumped through 6 mm i.d. Teflon™ tubing into the reservoir. The initial concentrations in the reservoir are listed in Table 3-4.

**Table 3-4.** Initial Liquid-Phase Tracer Concentrations in the Reservoir

Tracer	Initial Concentration (mg/L)
Acetone	100
Ethyl acetate	50
Toluene	17
Ethylbenzene	17
Cyclohexane	6.5

To reduce volatilization, care was taken to ensure that the tracers entered the reservoir below the water surface. During the spiking process, the mixing motor was activated in order to mix tracers throughout the reservoir volume. Adding the contents of the Tedlar™ bags increased the total liquid volume in the reservoir to 46 - 47 liters. This did not cause the 45 L reservoir to overflow, however, as some of the water simply entered the overlying glass channel.

Each experiment began as the process pump was activated at time zero. A stopwatch was started at the same instant. To facilitate additional mixing of tracers before sample

collection, the system was allowed to run for three to five minutes before the first samples were collected. During this lag period, the process pump was adjusted to the desired flowrate, and the discharge nozzle was aligned with the drain hub.

Usually, a total of ten liquid samples, including duplicates, were collected during each zone 2 experiment (Table 3-5). The final liquid sample was designated "L7," and was collected 64 minutes into the experiment. Before each liquid sample was collected, the stopcock on the side of the reservoir was opened for a few seconds in order to flush stagnant water from the sample line. A 20 mL glass crimp-top vial was then filled to approximately 10 mL from the same stopcock. Water would flow through the stopcock and through a short section of Teflon™ tubing attached to the outlet port of the stopcock. During sampling, this tubing was submerged inside the vial to minimize volatile losses. Immediately after sampling, the vial was sealed with an aluminum cap containing a Teflon™ lined septum.

**Table 3-5.** Liquid Sampling Schedule

Sample #	Sample Collection Times (minutes)
L1	4
LX	9
L2, L2D	14
L3	24
L4	34
L5, L5D	44
L6	54
L7	64

Duplicate liquid samples, designated in Table 3-5 by a "D," were collected at 14, and 44 minutes. Duplicates were typically collected no more than a few seconds after the primary sample. The sample "LX" was added during early trial experiments, when it was noticed that the more volatile tracers, particularly cyclohexane, would be largely absent by the end of the experiment. Taking an additional liquid sample early in the experiment resulted in a more defined concentration curve, i.e., to facilitate the calculation of mass transfer parameters.

Gas samples were also collected during all zone 2 experiments. A 6 mm i.d. Teflon™ tube extended into the throat of the downstream channel riser. Air was drawn through this tubing and into a Carbotrap™ 300 adsorbent tube, held in place by 6 mm i.d. Swagelok™

fittings. The air then passed through a bubble flowmeter (SKC Ultra-Flow Calibrator). Finally, the gas was conveyed through an air sampling pump (SKC PCXR8) and discharged into the ambient air. This configuration is shown on Figure 3-6.

The use of adsorbent tubes to collect gas samples is typically coupled with a check for chemical breakthrough, e.g., often based on some fraction of the gas samples being drawn through two tubes in series. For this study, preliminary experiments were completed to assess whether breakthrough would occur under worst-case experimental conditions. The tracers used in this study were added to a warm gas stream that was saturated with water vapor. The total moisture content, gas temperature and tracer concentrations were all greater than the highest values observed for this study and therefore reflect conditions that should be of greater concern with respect to breakthrough than any of the drain experiments described herein. As with drain experiments, the volume drawn through the adsorbent tubes ranged from 100 to 250 mL. In all cases the amount of mass appearing on breakthrough tubes (second in series) was less than method detection limits, and therefore less than 1% of total mass appearing on primary tubes. As such, it was concluded that for the gas volumes and concentrations used in this study, Carbotrap 300 tubes should be reliable without the employment of secondary breakthrough tubes.

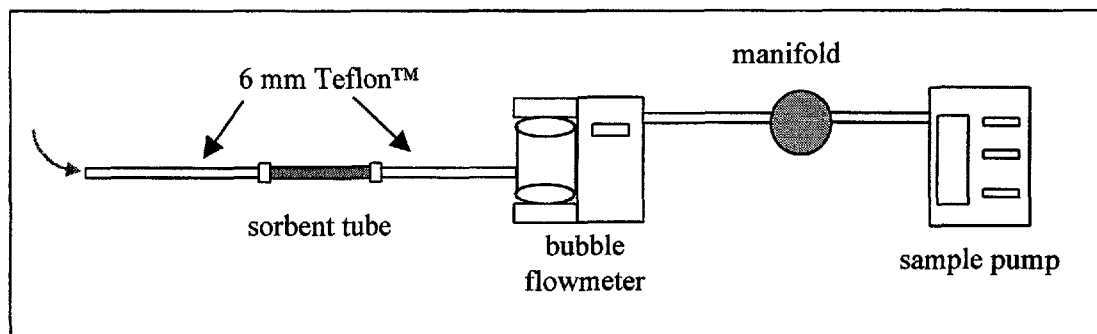


**Figure 3-6.** Gas Sampling Train

The timing of gas samples was planned such that the midpoint of the sampling period corresponded to the collection of a liquid sample. Actual sampling times ranged between 40 and 90 seconds. Therefore, a typical gas sampling period could commence 3 minutes and 30 seconds into the experiment and end about a minute later. Once the single gas sample had been collected, a glass cap was placed over the downstream drain riser, effectively sealing the

channel headspace. Between 100 and 250 mL of gas was conveyed through the sorbent tube while collecting a gas sample.

During the gas sampling process, multiple flow measurements were recorded using the bubble flowmeter. At least three air flow measurements were taken per sample. At the end of the sampling period, the pump was turned off. The sorbent tube was immediately removed from the sampling train and the ends sealed with 6 mm Swagelok™ end caps (with Teflon™ ferrules). Between gas samples, the sampling line was flushed of residual tracer. This was done by removing the sampling line from the channel riser, inserting a section of Teflon™ tubing in place of the sorbent tube, and operating the sampling pump for a period of time equal to or greater than the sample line residence time (usually about 15 seconds).

Seven gas samples were collected during each zone 2 experiment according to the schedule presented in Table 3-6. A gas sample blank was also collected; instead of drawing gas from the channel headspace, the air pump drew air from the environmental chamber.

**Table 3-6.** Gas Sampling Schedule for Zone 2 Experiments

Sample #	Sample Collection Midpoints (minutes)
G1	4
G2	14
G3	24
G4	34
G5	44
G6	54
G7	64

In addition to tracer samples, temperature and ventilation measurements were also taken during each experiment. Liquid temperature readings were taken using a digital dissolved oxygen (D.O.) meter (YSI Model 58) and probe. Every 10 minutes, the mixing motor was turned off and the D.O. probe was inserted into the reservoir. A steady temperature reading was always achieved within 5-10 seconds. The probe was then removed from the reservoir, the mixing motor was reactivated, and the temperature reading was recorded. Over the course of an experiment, the liquid temperature would rarely vary by more than one degree Celsius. Multiple air temperature readings were also taken during experiments, at 10 minute intervals. An Alnor™ Compuflow thermal anemometer (model #8565) was placed in

temperature mode and waved gently through the air. The average reading was then recorded. By switching the anemometer to velocity mode, velocities exiting the downstream riser could also be measured to a lower limit of 0.1 m/s. The anemometer probe was inserted into a sleeve placed over the downstream channel riser. By gently moving the probe across the riser cross-section, an average air speed was determined and recorded.

Channel depth was also measured near the end of each zone 2 experiment. As stated earlier, the depth of water in the channel was regulated by adding and removing plywood boards from underneath the reservoir. To ensure experimental consistency, the water depth was generally kept between 1 and 2.5 cm. To calculate this depth, the arc length of the non-wetted channel section was determined with a measuring tape. The water depth was then calculated based on channel geometry.

### Data Analysis (zone 2)

By the conclusion of each zone 2 experiment, the following data had been gathered for each chemical tracer: ten liquid concentration readings (primary and duplicate) and eight gas-phase concentration readings. Utilizing these data, the fractional stripping efficiencies and overall mass transfer coefficient ( $K_L A_c$ ) for all five chemical tracers were calculated.

When analyzing experimental data, it was appropriate to model the LDS as a well-mixed, recirculating batch reactor (Smith, 1981). During system operation, the majority of the tracer solution remained in the well-mixed reservoir; only a small fraction of it was in the piping or channel at any one time. Each time the water passed through the drain, a fraction of it would volatilize into the air. By analyzing the rate of volatilization, chemical-specific mass transfer properties were determined.

Integration of the appropriate mass balance for a batch reactor results in the following:

$$-\ln\left(\frac{C_1}{C_{10}}\right) = \eta_2 \frac{t}{\theta} = \eta_2 \tau \quad (3-3)$$

where:

$C_l$	=	liquid-phase concentration of the tracer (M/L <sup>3</sup> )
$C_{l0}$	=	initial liquid-phase concentration of the tracer (M/L <sup>3</sup> )
$\eta_2$	=	stripping efficiency for zone 2(-)
$t$	=	elapsed time of the experiment (T)
$\theta$	=	hydraulic residence time (V/Q <sub>l</sub> ) (T)
$V$	=	volume of liquid (L <sup>3</sup> )
$Q_l$	=	liquid flow rate (L <sup>3</sup> /T)
$\tau$	=	normalized time (t/θ) (-)

Plotting the negative natural logarithm of the normalized tracer concentration versus the normalized time results in a straight line, the "best fit" slope of which was equal to the tracer stripping efficiency. The average R<sup>2</sup> value over all zone 2 experiments and chemicals was 0.89. Average R<sup>2</sup> values ranged from 0.68 for acetone to 0.98 for cyclohexane.

An iterative method was used to determine K<sub>L</sub>A<sub>c</sub>. By modeling the liquid phase as a well-mixed batch reactor and the gas phase as a CFSTR, the following two mass balances were developed:

$$\frac{dC_l}{dt} = -\frac{K_L A_c}{V_l} \left( (1 - \eta_2) C_l - \frac{C_g}{H_c} \right) \quad (3-4)$$

$$\frac{dC_g}{dt} = \frac{K_L A_c}{V_g} \left( (1 - \eta_2) C_l - \frac{C_g}{H_c} \right) - \frac{Q_v C_g}{V_g} \quad (3-5)$$

where:

$C_l$	=	liquid-phase concentration of tracer (M/L <sup>3</sup> )
$C_g$	=	gas-phase concentration of tracer (M/L <sup>3</sup> )
$Q_l$	=	process flowrate (L <sup>3</sup> /T)
$V_l$	=	total liquid volume in the system (L <sup>3</sup> )
$V_g$	=	total volume of gas in the channel headspace (L <sup>3</sup> )
$Q_v$	=	ventilation rate of the channel headspace (L <sup>3</sup> /T)

- $K_L A_c$  = overall mass transfer coefficient for channel ( $L^3/T$ )
- $H_c$  = Henry's law constant for tracer ( $L^3liq/L^3gas$ )
- $\eta_2$  = stripping efficiency for zone 2 (-)
- $t$  = time (T)

Two initial conditions were required to solve Equations 3-4 and 3-5. The first condition was that the liquid-phase concentration at time = 0 was equal to the measured liquid-phase concentration from sample "L1", the first liquid sample collected in an experiment. The second condition was that the gas-phase concentration at time = 0 was equal to that measured from the initial gas sample. Equations 3-4 and 3-5 were then solved to give the following expressions for gas- and liquid-phase concentrations:

$$C_l = \frac{-DC_{go} + C_{lo}(m_2 + B)}{m_2 - m_1} e^{m_1 t} + \frac{DC_{go} - C_{lo}(m_1 + B)}{m_2 - m_1} e^{m_2 t} \quad (3-6)$$

$$C_g = \left[ \frac{-DC_{go} + C_{lo}(m_2 + B)}{m_2 - m_1} \right] \frac{m_1 e^{m_1 t}}{D} + \left[ \frac{DC_{go} - C_{lo}(m_1 + B)}{m_2 - m_1} \right] \frac{m_2 e^{m_2 t}}{D} + \frac{BC_l}{D} \quad (3-7)$$

where:

$$B = \frac{K_L A_c}{V_l} (1 - \eta_2)$$

$$D = \frac{K_L A_c}{V_l H_c} (1 - \eta_2)$$

$$E = \frac{K_L A_c}{V_g}$$

$$F = \frac{Q_v}{V_g} + \frac{K_L A_c}{V_g H_c}$$

$$m_1 = \frac{-(B + F) + \sqrt{(B + F)^2 - 4(BF - DE)}}{2}$$

$$m_2 = \frac{-(B + F) - \sqrt{(B + F)^2 - 4(BF - DE)}}{2}$$

$C_{go}$  = initial gas-phase concentration of tracer in the headspace ( $M/L^3$ )

$C_{lo}$  = initial liquid-phase concentration of tracer ( $M/L^3$ )

$K_L A_c$  = overall mass transfer coefficient for channel ( $L^3/T$ )

$V_l$  = total liquid volume in the system ( $L^3$ )

- $V_g$  = total volume of gas in the channel headspace ( $L^3$ )
- $Q_v$  = ventilation rate of the channel headspace ( $L^3/T$ )
- $H_c$  = Henry's law constant for tracer ( $L^3_{liq}/L^3_{gas}$ )
- $t$  = time (T)

The mass transfer coefficient  $K_L A_c$  is embedded within the terms B, D, E, and F. By inserting known experimental parameters ( $C_{g0}$ ,  $C_{l0}$ ,  $Q_v$ , etc.) and estimating  $K_L A_c$ , Equation 3-6 was used to predict liquid-phase tracer concentrations. These estimated concentrations were then compared to measured liquid concentrations. By adjusting the  $K_L A_c$  value, it was possible to minimize the sum of squared relative residuals between the predicted and actual liquid-phase concentrations:

$$R_T = \sum_{i=1}^n \left[ \frac{(C_m - C_p)}{C_m} \right]^2 \tag{3-8}$$

where:

- $R_T$  = sum of the squared relative residuals (-)
- $C_m$  = measured concentration ( $M/L^3$ )
- $C_p$  = predicted concentration ( $M/L^3$ )

The minimum residual was used to determine  $K_L A_c$  for each tracer and experiment.

Values of  $K_L A_c$  are only applicable for the tracers for which they have been calculated. However, by determining individual liquid- and gas-phase mass transfer coefficients ( $k_g A_c$  and  $k_l A_c$ ), it is possible to calculate  $K_L A_c$  for any chemical given the Henry's law constant for that chemical. As well as gaining a new insight on the mechanisms responsible for mass transfer, deriving values of  $k_l A_c$  and  $k_g A_c$  was a necessary step in developing empirical correlations.

In this study,  $k_l A_c$  and  $k_g A_c$  were calculated by comparing  $K_L A_c$  ratios. The first step involved a determination of  $k_g/k_l$ . Figure 3-7 is a matrix whose cells consist of ratios of  $K_L A_c$  values for the tracer of that row and the tracer of that column. For example, the element in the third row and second column of the matrix is equal to the  $K_L A_c$  for toluene divided by the  $K_L A_c$  for ethyl acetate.

	Acetone	Ethyl Acetate	Toluene	Ethylbenzene	Cyclohexane
Acetone	1	$K_L(A)/K_L(EA)$	$K_L(A)/K_L(T)$	$K_L(A)/K_L(EB)$	$K_L(A)/K_L(C)$
Ethyl acetate	$K_L(EA)/K_L(A)$	1	$K_L(EA)/K_L(T)$	$K_L(EA)/K_L(EB)$	$K_L(EA)/K_L(C)$
Toluene	$K_L(T)/K_L(A)$	$K_L(T)/K_L(EA)$	1	$K_L(T)/K_L(EB)$	$K_L(T)/K_L(C)$
Ethylbenzene	$K_L(EB)/K_L(A)$	$K_L(EB)/K_L(EA)$	$K_L(EB)/K_L(T)$	1	$K_L(EB)/K_L(C)$
Cyclohexane	$K_L(C)/K_L(A)$	$K_L(C)/K_L(EA)$	$K_L(C)/K_L(T)$	$K_L(C)/K_L(EB)$	1

**Figure 3-7.**  $K_L A_c$  Matrix Used to Determine  $k_g/k_l$  Ratios.

Each set of experimental conditions had its own unique matrix. A second matrix is then constructed, similar in structure to the first, but containing predicted  $K_L A_c$  ratios. Predicted ratios were calculated using Equation 3-9, in which the ratio of gas to liquid-phase mass transfer coefficients ( $k_g/k_l$ ) is a key variable (Howard *et al.*, 1996):

$$\frac{K_{Li} A_c}{K_{Lj} A_c} = \Psi_l \Psi_g \left\{ \begin{matrix} H_{ci} \\ H_{cj} \end{matrix} \right\} \left\{ \frac{1 + \left[ \frac{k_{gj}}{k_{lj}} \right] H_{cj}}{\Psi_l + \Psi_g H_{ci} \left[ \frac{k_{gj}}{k_{lj}} \right]} \right\} \quad (3-9)$$

where:

- $K_{Li} A_c$  = overall mass transfer coefficient for chemical i ( $L^3/T$ )
- $K_{Lj} A_c$  = overall mass transfer coefficient for chemical j ( $L^3/T$ )
- $k_{gj}$  = gas-phase mass transfer coefficient for chemical j ( $L/T$ )
- $k_{lj}$  = liquid-phase mass transfer coefficient for chemical j ( $L/T$ )
- $H_{ci}$  = Henry's law constant for chemical i ( $L^3_{liq}/L^3_{gas}$ )
- $H_{cj}$  = Henry's law constant for chemical j ( $L^3_{liq}/L^3_{gas}$ )
- $\Psi_l, \Psi_g$  = mass transfer proportionality constants (eq. 2-3 and 2-4) (-)

By adjusting the  $k_g/k_l$  ratio, the sum of the squared residuals between the experimental and predicted matrices was minimized. For their use in  $\Psi_l$  and  $\Psi_g$ , the diffusivity exponents n and m (Equations 2-3 and 2-4) were assigned a value of 2/3 (a commonly accepted compromise between two-film and penetration theories) (Munz and Roberts, 1989).

For any experiment, the values of  $k_g/k_l$  should vary only slightly between volatile chemicals, an assumption that was made for this study. Once the ratio had been determined,  $k_l A_c$  and  $k_g A_c$  were determined from Equations 3-10 and 3-11:

$$k_l A_c = \frac{K_L A_c \left[ \left( \frac{k_g}{k_l} \right) H_c + 1 \right]}{\left( \frac{k_g}{k_l} \right) H_c} \quad (3-10)$$

$$k_g A_c = \left( \frac{k_g}{k_l} \right) k_l A_c \quad (3-11)$$

where:

- $k_l A_c$  = liquid-phase mass transfer coefficient for channel ( $L^3/T$ )
- $k_g A_c$  = gas-phase mass transfer coefficient for channel ( $L^3/T$ )
- $K_L A_c$  = overall mass transfer coefficient for channel ( $L^3/T$ )
- $k_g/k_l$  = ratio of gas to liquid phase mass transfer coefficients (-)
- $H_c$  = Henry's law constant for chemical of interest ( $L^3_{liq}/L^3_{gas}$ )

## ZONE 1 ANALYSIS

A total of 64 experiments (including duplicates) were completed to better understand the mechanisms associated with emissions from water seals. Important zone 1 mass transfer parameters included the rate at which air bubbles are entrained in the water seal ( $Q_e$ ), the degree of equilibrium reached by bubbles within the water seal ( $\gamma$ ), and the gas- and liquid-phase mass transfer coefficients associated with surface volatilization ( $k_l A_s$  and  $k_g A_s$ ).

### Experimental System (zone 1)

Both the trap simulators and the LDS were used to determine zone 1 emission parameters. For experiments completed with a trap simulator, the liquid flowrate dictated which plexiglass cap, glass cylinder, and PVC collar were to be used. For intact falling films, the smallest glass cylinder was usually adequate for capturing the entire process flow. However, when the falling film was disintegrated, a larger cylinder was required to prevent excessive process flow spillage. The necessary PVC collar length decreased as the liquid film

transitioned from disintegrated to solid flow regimes, but would then lengthen with increasing liquid flow. By adding and removing plywood spacer boards from underneath the trap simulator, the length of the falling film was controlled. Depending on the liquid flowrate, film lengths ranged between 30 and 33 cm. During experiments to determine the air entrainment rate, the glass reservoir was not used. Instead, water was pumped from a nearby wash basin, run through the trap and discharged back into the basin. This allowed experiments to continue for as long as needed.

During experiments completed using the LDS, a glass J-trap was attached to the drain riser. In several cases, the wind tunnel was also used to simulate the effects of wind blowing over the drain hub. During LDS zone 1 experiments, the total falling film and its exposed length were fixed at 31 and 10 cm, respectively.

**Experimental Plan and Methodology (zone 1)**

The goal of zone 1 experiments was the calculation of several key emission parameters: the air entrainment rate in a water trap ( $Q_a$ ), the degree of equilibrium for entrained bubbles ( $\gamma$ ), and the mass transfer coefficient for surface volatilization ( $K_L A_s$ ). As with zone 2, the experiments were designed so that the different emission mechanisms could be isolated and quantified. A total of 40 experiments were completed to measure  $Q_a$  using the trap simulators described previously. A summary of zone 1 entrainment experiments is presented in Table 3-7.

**Table 3-7. Summary of Air Entrainment Experiments**

Disintegrated Falling Film			Intact Falling Film		
Experiments	Trap i.d. (cm)	Liquid flowrate (L/min)	Experiments	Trap i.d. (cm)	Liquid flowrate (L/min)
E1-E2	10	3.8	E21	10	7.6
E3-E6	10	5.7	E22-E23	10	9.5
E7-E11	10	7.6	E24-E27	10	11.4
E12-E14	10	9.5	E28-E29	10	13.2
E15	7.6	3.8	E30-E32	10	15.1
E16-E17	7.6	5.7	E33-E34	10	16.3
E18-E19	7.6	7.6	E35	7.6	9.5
E20	7.6	9.5	E36	7.6	11.4
			E37-E38	7.6	13.2
			E39-E40	7.6	15.1

Certain process flowrates were associated with both disintegrated and intact (solid) falling liquid films. For the piping arrangement used in this study, the transition between disintegrated and intact flow typically occurred at a process flowrate of about 10.6 L/min. However, it was observed that under some conditions, an intact falling film could exist at flowrates as low as 7 L/min.

A total of 24 experiments were performed with the objective of determining mass transfer parameters ( $Q_e$ ,  $\gamma$ ,  $k_f A_s$ ,  $k_g A_s$ ) associated with emission mechanisms in the water seal. The first set of these experiments was completed using trap simulators. The results were used to determine values of  $Q_e$  and  $\gamma$ . A summary of these experiments is provided in Table 3-8. Both liquid flowrate and trap diameter were considered as possible factors contributing to bubble-induced mass transfer.

**Table 3-8. Summary of Bubble Mass Transfer Experiments**

Expt. #	Trap Simulator Diameter (cm)	Liquid Flowrate (L/min)	T <sub>liq</sub> (°C)	Flow Profile
B1	5	7.6	22.2	Disintegrated
B2	5	9.5	22.9	Disintegrated
B3	5	11.4	23.2	Intact
B4	5	15.1	22.5	Intact
B5	7.6	5.7	22.6	Disintegrated
B6	7.6	7.6	22.8	Disintegrated
B7	7.6	9.5	23.2	Disintegrated
B8	7.6	11.4	24	Intact
B8-B	7.6	11.4	23.3	Intact
B9	7.6	15.1	24	Intact
B9-B	7.6	15.1	23.2	Intact
B10	10	5.7	24.3	Disintegrated
B11	10	7.6	24.3	Disintegrated
B12	10	9.5	22.7	Disintegrated
B13	10	11.4	24.3	Intact
B14	10	15.1	24	Intact
B14-B	10	15.1	22.5	Intact

The next set of experiments was dedicated to determining mass transfer coefficients due to surface volatilization at the water seal. These experiments were completed using the LDS. The system was prepared by attaching the 5 cm J-trap to the drain riser. In several

cases, the wind tunnel was also used. Variables expected to affect  $k_p A_s$  and  $k_g A_s$  included process flowrate and the absence or presence of wind over the drain hub. A summary of surface volatilization experiments is provided in Table 3-9.

**Table 3-9.** Summary of Surface Volatilization Experiments

Expt. #	Liquid Flowrate (L/min)	T <sub>liq</sub> (°C)	Wind Velocity (m/s)	Flow Profile
S1	3.8	23.7	0	Disintegrated
S2	7.6	23.8	0	Disintegrated
S3	7.6	21.8	1.62	Disintegrated
S4	7.6	24.8	2.75	Disintegrated
S5	11.4	23.5	0	Intact
S6	15.1	24.2	0	Intact
S7	15.1	21.7	2.73	Intact

No chemical tracers were used during  $Q_o$  experiments. The appropriate collar, cap and glass cylinder were first fitted to the upstream connection of the trap. Non-hardening putty, applied only to the exterior of the trap, was used to seal the components. The process pump was activated and the trap simulator was manually shifted such that the process flow was properly aligned with the glass cylinder. It was possible to observe the water surface through the plexiglass cap. This allowed the glass cylinder to be adjusted such that it extended just below the water surface. A Tedlar™ bag was attached to the gas sampling port built into the cap. This bag was then opened, and a stopwatch was started. The bag was then allowed to inflate. The length of the sampling period depended on the entrainment rate in the trap; sample collection times ranged between 30 seconds and 2.5 minutes. For an accurate measurement, at least several hundred milliliters of air were required. Conversely, it was undesirable to capture more than 1.5 liters in the bag. An overly full sample bag could lead to such an increase in the headspace pressure that the liquid surface would be pushed down, possibly exposing the bottom edge of the glass cylinder. When sampling was complete, the Tedlar™ bag was sealed and disconnected from the sample port. It was then attached to a gas sampling train very similar to that on Figure 3-6, the only difference being that there was no adsorbent tube. The bag was reopened, and a sample pump (SKC PCXR8) was used to evacuate its contents. Multiple flowmeter measurements were recorded before the bag completely emptied. Flow measurements generally varied by less than 5% during any experiment. An average value was used for all analyses.

Experiments to determine the degree of equilibrium reached by entrained air bubbles ( $\gamma$ ) were conducted in a manner very similar to that used during  $Q_e$  experiments. However,  $\gamma$  experiments involved the use of liquid tracers. Tracer solutions were prepared according to the methods described previously. They were then spiked into the glass reservoir just as they were during zone 2 experiments. Once this was completed the mixing motor was operated for approximately 5 minutes. This extended time was necessary to ensure a uniform tracer concentration in the reservoir; unlike experiments with the LDS, there was no tracer recirculation to facilitate mixing. Liquid and air temperature measurements were taken, using the D.O. meter and anemometer described previously. The next step involved collection of two liquid samples from the reservoir. The mixing motor was then turned off and the process pump was started. Approximately 30 seconds after the pump was started, an additional liquid sample was collected from the reservoir. Depending on the liquid flowrate, another 30 to 90 seconds was then allowed to pass before the collection of the first trap sample. This lag time was intended to allow steady-state conditions to be established in the trap and headspace. Once this period had passed, four to five samples were collected, at regular intervals, from the stopcock mounted in the side of the trap simulator. Gas samples were collected in a manner similar to the  $Q_e$  experiments. Immediately following an experiment, the Tedlar™ bag containing the sample gas was attached to a gas sample train identical to that on Figure 3-6. Several sorbent tube samples were collected from this gas volume.

### Data Analysis (zone 1)

The following equation was used to calculate the rate, in liters/min, at which air was entrained within a water seal:

$$Q_e = \frac{Q_{\text{empty}} t_{\text{empty}} + \sum_{i=1}^n Q_s t_s}{t_{\text{fill}}} \quad (3-12)$$

where:

- $Q_e$  = air entrainment rate ( $L^3/T$ )
- $Q_{\text{empty}}$  = average gas flowrate during bag evacuation ( $L^3/T$ )
- $t_{\text{empty}}$  = time required to completely evacuate sample bag (T)

$Q_s$	=	average gas flowrate when sampling through sorbent tube ( $L^3/T$ )
$t_s$	=	duration of sorbent tube sample collection (T)
$n$	=	number of gas samples collected (-)
$t_{fill}$	=	time required to fill sample bag (T)

During experiments, it was observed that the presence of the glass cylinder in the trap simulator greatly suppressed the amount of splashing which occurred at the water seal. With the exception of minor disturbances caused by rupturing air bubbles, the enclosed water seal surface was quiescent. However, the presence of the glass cylinder appeared to have no discernable affect on the magnitude or pattern of air entrainment. This observation formed the foundation of an important assumption which allowed zone 1 emission mechanisms to be isolated from one another. During experiments using the trap simulator, it was assumed that all of the mass transfer was due to bubble entrainment, with surface volatilization playing a negligible role.

The extent of chemical equilibrium in the bubbles,  $\gamma$ , was simply calculated by dividing the average measured gas concentration by the product of the average measured liquid-phase trap concentration and the Henry's law constant:

$$\gamma = \frac{C_g}{C_l H_c} \quad (3-13)$$

where:

$\gamma$	=	degree of equilibrium of entrained air bubbles (-)
$C_g$	=	tracer concentration in simulator headspace ( $M/L^3$ )
$C_l$	=	tracer concentration in simulator water seal ( $M/L^3$ )
$H_c$	=	Henry's law constant for a tracer ( $L^3_{liq}/L^3_{gas}$ )

Using measured values for  $Q_e$  and  $\gamma$ , a stripping efficiency due solely to entrained air was estimated. This stripping efficiency ( $\eta_b$ ) was then compared with zone 1 stripping efficiencies ( $\eta_1$ ) for Experiments S1 through S7. The difference was attributed to surface volatilization in accordance with Equations 3-14 and 3-15. Equation 3-15 was used to determine overall mass transfer coefficients due to surface volatilization and is based on the

solution of Equation 2-5 where  $\eta_1$  is replaced by  $\eta_s$  and the bubble entrainment term ( $Q_e H_{c, \gamma} / Q_i$ ) is set equal to zero.

$$\eta_s = \eta_1 - \eta_b \quad (3-14)$$

$$K_L A_s = \frac{Q_i}{1 - \eta_s} - Q_i \quad (3-15)$$

where:

- $\eta_s$  = stripping efficiency due solely to surface volatilization (-)
- $\eta_1$  = total stripping efficiency for zone 1 (-)
- $\eta_b$  = stripping efficiency due solely to bubbles (-)
- $K_L A_s$  = overall mass transfer coefficient for surface volatilization ( $L^3/T$ )
- $Q_i$  = liquid flowrate through the trap ( $L^3/T$ )

The surface volatilization mechanism was divided into its individual liquid ( $k_l A_s$ ) and gas ( $k_g A_s$ ) components using the exact same matrix method as was used for zone 2.

## QUALITY ASSURANCE

To verify the integrity of experimental and analytical equipment and methodologies, a series of quality assurance measures was undertaken. For this study, the quality assurance program included: the development of equipment calibration curves, the determination of method detection limits, mass closure analysis, analysis of duplicate samples, analysis of sample blanks, and completion of four replicate experiments.

During sample analysis, five-point liquid and gas calibration curves were prepared for each volatile tracer. Liquid standards were prepared in 20 mL glass crimp-top vials. The first step was to pipette 10 mL of deionized water into each vial. These vials were then capped with aluminum caps containing Teflon™-lined septa. Glass gas-tight syringes (Hamilton) were then used to withdraw known quantities of tracer solution from a Tedlar™ standard bag. Through a single piercing of the septum, this stock standard was then injected into each standard vial. A summary of the volumes added, and the resulting concentrations in each standard vial is provided in Table 3-10.

The standard designated "3D" was not used in the development of the calibration curve. Instead, it was used to perform a "midpoint check." During GC analysis, the standard vials were generally the first to be analyzed. They would then be followed by experimental samples and blanks. Vial "3D" was analyzed last. Its purpose was to verify the quality of the calibration curve and to detect any drift that may have occurred in the GC response.

**Table 3-10.** Analytical Liquid Standards Prepared from Tedlar™ Bag #7

Standard #	Amount From Bag	Expected Concentration (mg/L)				
		Acetone	Ethyl Acetate	Toluene	Ethylbenzene	Cyclohexane
1	1.6 mL	108.1	57.4	14.3	14.3	7.4
2	800 µL	58.0	30.8	7.7	7.7	4.0
3, 3D	500 µL	37.3	19.8	4.9	4.9	2.5
4	250 µL	19.1	10.1	2.5	2.5	1.3
5	50 µL	3.9	2.1	0.5	0.5	0.3

Gas standards were drawn from a certified custom gas standards cylinder prepared by Scott Specialty Gases, Inc. Gas concentrations were gravimetrically certified with an analytical accuracy of 2%. Tracer concentrations are listed in Table 3-11.

**Table 3-11.** Concentrations of Scott Specialty Gases Standards Cylinder

Compound	Concentration
Acetone	40.0 ppmv
Ethyl Acetate	50.6 ppmv
Toluene	40.5 ppmv
Ethylbenzene	27.7 ppmv
Cyclohexane	19.9 ppmv
Air	Balance

The cylinder regulator was opened and a small volume of standards gas was allowed to flow into a 3 L Tedlar™ bag. This bag was then attached to a gas sampling train similar to the one on Figure 3-6. Immediately after activating the sampling pump, a gas flowmeter measurement was taken. Gas was then allowed to flow through a standards tube until such time that the desired tracer mass had been deposited on the adsorbent. Table 3-12 summarizes the gas volumes and tracer masses drawn through each standards tube.

**Table 3-12.** Analytical Gas Standards Prepared from Scott Specialty Gases Cylinder

Standard #	Volume Through Tube	Mass Deposited on Sorbent Tube (µg)				
		Acetone	Ethyl Acetate	Toluene	Ethylbenzene	Cyclohexane
1	800 mL	76.8	147.3	123.2	97.2	55.4
2	500 mL	48.0	92.1	77.0	60.8	34.6
3	400 mL	38.4	73.7	61.6	48.6	27.7
4	150 mL	14.4	27.6	23.1	18.2	10.4
5	50 mL	4.8	9.2	7.7	6.1	3.5

Over the course of 38 mass transfer experiments, a total of 17 liquid and gas calibration curves were developed for each chemical tracer. Calibration curves were consistently linear in nature, with typical coefficients of determination ( $R^2$ ) exceeding 0.99. Average response deviations between the vial "S3D" and the calibration curve ranged between 3.2% for acetone to 10.2% for cyclohexane.

A method detection limit (MDL) represents the smallest amount of an analyte that can be reliably detected above the random background noise present in the analysis of blanks (Berthouex, 1994). To determine MDLs for both liquid and gas analysis methods, a number of identical samples were prepared and analyzed. Liquid MDLs were based on 13 identically prepared liquid samples in accordance with the method of Simes (1991). For each, 500 µL was drawn from a Tedlar™ standards bag and injected into a vial already containing 10 mL of deionized water. For gas MDLs, 300 mL of standards gas was drawn through eight different sorbent tubes. Once these samples were analyzed, the standard deviation of the GC responses was determined and Equation 3-16 was used to derive the MDL:

$$MDL = t(n-1, 1-\alpha)s, \quad (3-16)$$

where:

MDL = method detection limit (GC response)

t = one sided t-distribution

- n = number of samples analyzed (-)  
 $\alpha$  = confidence level (99% in this case)  
 $s_r$  = standard deviation of the GC peak areas (GC response)

In the case of the liquid sample population, the one sided t distribution,  $t(12,0.99)$  was equal to 2.681 while for the group of gas samples,  $t(7,0.99)$  was equal to 2.998. Calculated MDLs are listed in Table 3-13.

**Table 3-13.** Liquid- and Gas-Phase Method Detection Limits (MDLs)

Chemical	Liquid-Phase MDL (mg/L)	Gas-Phase MDL ( $\mu\text{g}$ )
Acetone	1.5	1.8
Ethyl Acetate	0.7	5.9
Toluene	0.4	4.1
Ethylbenzene	0.6	6.9
Cyclohexane	0.3	0.2

Due to its high volatility, cyclohexane was the only chemical tracer whose liquid-phase concentration would regularly drop below its MDL. Near the end of certain experiments, concentrations as low as 0.1 mg/L were observed. Therefore, when determining overall mass transfer coefficients for cyclohexane, any measured liquid concentrations below 0.3 mg/L were disregarded. Even after these low values were removed there were still at least five valid cyclohexane concentrations that were used to calculate  $K_L A$ .

As calculated, gas-phase MDLs were always lower than the sample masses collected during all trap simulator and most LDS experiments. However, in several LDS experiments, measured masses of toluene, ethylbenzene and cyclohexane collected on the sorbent tube were significantly below the MDL values listed in Table 3-13. Also, when collecting gas sample blanks, the collected tracer masses for all compounds were typically lower than their calculated MDL. During LDS experiments, only the results of the initial gas sample were utilized when determining mass transfer coefficients. In all cases, the measured tracer masses on this first sample were above the MDL.

An assessment of mass closure is a valuable tool for assessing the quality of experimental data and identifying undesirable sources and sinks. In this study, a mass closure analysis was conducted in every mass transfer experiment where it was deemed feasible (where the gaseous flowrate and concentration could be ascertained). These included all experiments with the trap simulators, and zone 2 experiments completed with the LDS. The only mass transfer experiments where no mass closure was attempted were LDS experiments involving above-trap emissions, and S1 through S7.

The degree of mass closure was reported as a mass recovery, expressed in percent. The mass recovery was calculated using Equation 3-17:

$$m_c = 100 \left( \frac{m_{out}}{m_{in}} \right) = 100 \left( \frac{V_l C_l + m_g}{V_l C_{l_0}} \right) \quad (3-17)$$

where:

$m_c$	=	mass recovery (%)
$m_{in}$	=	total mass entering the system (M)
$m_{out}$	=	total mass leaving the system (M)
$m_g$	=	total mass leaving the system in the gas phase (M)
$V_l$	=	liquid volume (L <sup>3</sup> )
$C_{l_0}$	=	concentration of tracer entering system in the liquid phase (M/L <sup>3</sup> )
$C_l$	=	concentration of tracer exiting system in the liquid phase (M/L <sup>3</sup> )

With the LDS, the mass entering the system was calculated by multiplying the initial liquid-phase concentration by the total liquid volume. The liquid-phase mass "exiting" the system was defined as the mass of liquid-phase tracer remaining at the end of an experiment (final concentration multiplied by total volume). In experiments using a trap simulator, the entering mass was equal to the initial liquid volume in the reservoir multiplied by the average measured reservoir concentration. Liquid-phase "exiting" mass was equal to the product of the initial liquid volume in the reservoir and the average liquid-phase concentration in the trap.

It was assumed that no tracer mass entered the system in the gas phase. In the LDS, the rate at which gas-phase tracer left the system changed with time. Therefore, to determine the total mass leaving the system in the gas phase, the mass flowrate had to be integrated over the duration of the experiment. This was done by constructing a series of trapezoids, the sides of which corresponded to gas samples. Figure 3-8 illustrates this concept.

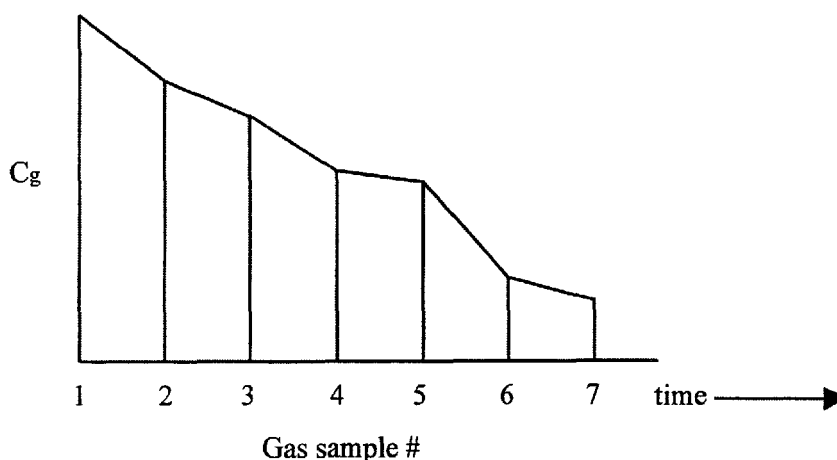


**Figure 3-8.** Estimating the Mass of Gas-Phase Tracer Leaving the LDS

The next step was to determine the product of the total trapezoid area and the headspace ventilation rate. Residual gas existing in the headspace at the end of an experiment was also accounted for in the total mass. The resulting expression (Equation 3-18) was used to calculate the total mass of gas-phase tracer which “exited” the system:

$$m_g = V_g C_{g(n)} + Q_v \sum_{i=1}^{n-1} \left( \frac{C_{g(i)} + C_{g(i+1)}}{2} \right) t_s \tag{3-18}$$

where:

- $m_g$  = total mass leaving the system in the gas phase (M)
- $V_g$  = headspace volume ( $L^3$ )
- $C_{g(i)}$  = measured gas concentration of sample  $i$  ( $M/L^3$ )
- $C_{g(n)}$  = measured gas concentration in headspace at end of experiment ( $M/L^3$ )
- $Q_v$  = ventilation rate in the channel headspace ( $L^3/T$ )
- $n$  = number of gas samples collected during experiment (-)
- $t_s$  = interval between gas samples (T)

In experiments completed with a trap simulator, the total mass of gas-phase tracer leaving the system was determined according to Equation 3-19:

$$m_g = C_g(Q_e t_e + V_H) \tag{3-19}$$

where:

- $m_g$  = total mass leaving the system in the gas phase (M)
- $t_e$  = duration of experiment (T)
- $V_H$  = volume of trap simulator headspace ( $L^3$ )
- $Q_e$  = bubble entrainment rate ( $L^3/T$ )
- $C_g$  = steady-state gas concentration exiting system ( $M/L^3$ )

Typical trap simulator headspace volumes were approximately 200 - 300 mL.

The results of the mass closure analysis are presented in Table 3-14.

**Table 3-14. Mass Closure Analysis**

Tracer	Mass Recoveries (%)					
	Experiments B1-B14B			Experiments C1-C11		
	Low	High	Avg.	Low	High	Avg.
Acetone	96	103	100	94	111	102
Ethyl Acetate	97	103	100	94	143	118
Toluene	73	125	97	63	117	89
Ethylbenzene	72	127	97	55	126	74
Cyclohexane	57	139	88	39	83	52

Without exception, higher volatility chemicals were associated with lower and more scattered mass recoveries. Incidental tracer losses may be responsible for these lower values. Sorption and volatilization from the reservoir are two possible tracer sinks; both mechanisms are more significant for the higher volatility compounds used in this study. In the LDS, it is possible that ventilation short-circuiting resulted in lower mass recoveries. While an air stream may quickly pass through the channel headspace and exit the downstream riser, there may be parcels of stagnant air at the upstream and downstream ends of the sewer reach.

As illustrated in Table 3-14, mass recoveries for trap simulator experiments were generally closer to 100% than those from LDS experiments. Because of their short duration, trap simulator experiments were characterized by significantly less tracer volatilization than their LDS counterparts. From Equation 3-17, this larger final liquid concentration results in a larger mass recovery value, regardless of the gas sampling quality.

Duplicate samples and replicate experiments were also used to evaluate experimental quality. Depending on its duration, 2, 3, or 4 duplicate liquid samples were collected during each LDS experiment, with an average duplication rate of 25%. Replicate experiments were also completed. In this study, Experiments B8, B9, B14, and C2 were repeated. When completing duplicate experiments, every effort was made to ensure similarity with the original experiments. Nevertheless, there were usually minor differences between the duplicate and the original, the most common being with the liquid and air temperatures.

The average deviation between duplicate liquid samples ranged from 2.4% for ethyl acetate to 11.5% for cyclohexane. These deviations would be somewhat smaller were it not for the extremely large GC response difference recorded for the first duplicate sample of Experiment C2. After Experiment C2, the mixing motor was installed and duplicate precision improved considerably. Generally, duplicate sample quality increased as an experiment progressed, indicating that reservoir tracer concentrations became more uniform over time.

Sample blanks were a valuable means of confirming equipment performance and experimental assumptions. In this study, three categories of sample blanks were defined. The first were liquid blanks. These were simply crimp-top vials filled with 10 mL of tap water. During sample analysis, one blank was analyzed for every 6 to 10 normal samples. By observing the chromatographs of these blank samples, it could be determined whether any sample transfer lines had been contaminated with residual organics from previous analyses. Gas blanks were used for the same purpose. A hollow steel tube was placed in the thermal desorber. This tube was analyzed after every six samples, transporting any organic residuals through the FID. Experimental gas blanks were the third type of sample blank. These were collected during experiments with the LDS. Unlike other gas samples, the air drawn through the blank tube was not from the downstream riser throat, but from the ambient air in the environmental chamber. These blanks ensured that ambient gas-phase tracer concentrations

were much lower than those in the channel headspace, and confirmed the assumption that air entering the drain riser was largely devoid of tracer contamination. During all mass transfer experiments, measured sample blank concentrations were less than 5% of the concentrations observed during the next normal sample.

## 4. EXPERIMENTAL RESULTS

The experiments described in Chapter 3 led to an experimental database that allowed for the development of mathematical correlations between several variables and system parameters. Relevant correlations are presented in this chapter. Where appropriate, correlations are preceded by additional discussion of research findings.

### ZONE 1

Within the water seal, both air entrainment and surface volatilization were considered as possible emission mechanisms. As described in Chapter 3, by using the results of two sets of experiments (trap simulator and LDS), fractional stripping efficiencies and mass transfer parameters were determined.

#### **Experimental Results: Stripping Efficiencies**

Trap simulator experiments were completed with the goal of estimating stripping efficiencies, air entrainment rates, and the degree of equilibrium achieved by entrained air bubbles. By collecting liquid samples from both the reservoir and the trap, it was hoped that stripping efficiencies could be calculated directly from liquid-phase data. Unfortunately, when these data were analyzed the resulting stripping efficiencies were highly scattered, precluding their use to determine mass transfer parameters. Thus, stripping efficiencies attributed to entrained air bubbles ( $\eta_b$  in Equation 3-14) were calculated from two measured experimental values: the degree of equilibrium of entrained air bubbles and the volumetric rate at which air was entrained in the trap. By substituting measured  $\gamma$  and  $Q_e$  values into Equation 2-5, predicted bubble stripping efficiencies were calculated. These are presented in Table 4-1.

For all three trap simulator sizes (5 cm, 7.6 cm, 10 cm i.d.) stripping efficiencies due to bubbles decreased sharply as the process flow moved from a disintegrated profile to a smooth profile (between 9.5 and 11.4 L/min). The primary reason for this drop was that the solid falling films entrained much less air than disintegrated ones due to their smaller surface to volume ratios.

Except for Experiments B10 through B12, where no trend was apparent, during most disintegrated film experiments the stripping efficiency associated with bubbles decreased as the process flowrate increased. In part, this result is due to shorter hydraulic residence times in the water seal at higher liquid flowrates. Even though both 5.7 and 9.5 L/min films were considered disintegrated, falling films corresponding to the lower flowrates were also more dispersed, i.e., characterized by liquid droplets and internal air parcels. These dispersed films generated air entrainment rates nearly as high as those from the larger disintegrated flowrates. Generally, the opposite phenomenon occurred with intact (solid) falling films. As the process flow increased, the bubble stripping efficiency also increased. This was directly related to the higher entrainment rates observed with the larger intact films.

To isolate the effect of surface volatilization, experiments S1 through S7 were completed with the LDS. These experiments were completed without any obstructions which could suppress splashing. Since experiments were completed with a water seal, the channel section reached a condition of dynamic equilibrium for all tracers with the exception of cyclohexane. As such, all of the stripping efficiencies listed in Table 4-2, with the exception of those for cyclohexane, should correspond to zone 1 ( $\eta_1$  in Equation 3-14). Values of  $\eta_b$  based on B-series experiments (Table 4-1) were subtracted from values of  $\eta_1$  based on S-series experiments (Table 4-2) for similar operating conditions to obtain values of  $\eta_s$  (stripping efficiencies due to surface volatilization). Resulting values of  $\eta_s$  are presented in Table 4-3.

Among experiments involving a disintegrated film (S1 through S4), the greatest values of  $\eta_1$  and  $\eta_s$  occurred at the 3.8 L/min liquid flowrate, the lowest used in this study. Values of  $\eta_1$  for all tracers but cyclohexane then sharply decreased for Experiment S2, performed at 7.6 L/min. In part, this is due to a longer trap residence time during low-flow experiments. It is also possible that drain throat ventilation rates changed significantly with changing liquid flowrates, i.e., greater ventilation rates due to the larger surface-to-volume ratios associated with low process flows. The anomaly for cyclohexane was likely due to continued mass transfer in the underlying channel.

**Table 4-1.** Stripping Efficiencies Due to Entrained Air Bubbles ( $\eta_b$ )

Expt. #	Liquid Flowrate (L/min)	Stripping Efficiencies (%)				
		Acetone	Ethyl Acetate	Toluene	Ethylbenzene	Cyclohexane
B1	7.6	0	0.1	2.8	2.3	8.6
B2	9.5	0	0	2.1	1.8	6.1
B3	11.4	0	0	0.5	0.4	2.3
B4	15.1	0	0	0.6	0.5	1.7
B5	5.7	0	0.1	4.4	3.6	9.9
B6	7.6	0	0.1	3.6	2.9	11.1
B7	9.5	0	0.1	3.5	2.9	9.3
B8	11.4	0	0	0.6	0.5	1.2
B8-B	11.4	0	0	0.5	0.4	1.6
B9	15.1	0	0	1.0	0.9	2.6
B9-B	15.1	0	0	1.1	1.0	5.0
B10	5.7	0	0.1	3.4	2.6	5.0
B11	7.6	0	0.1	3.1	2.4	6.2
B12	9.5	0	0.1	3.3	2.7	8.2
B13	11.4	0	0	0.8	0.6	2.4
B14	15.1	0	0	1.1	0.9	3.6
B14-B	15.1	0	0	1.0	0.8	3.2

B1-B4 = 5 cm trap simulator  
 B5-B9B = 7.6 cm trap simulator  
 B10-B14B = 10 cm trap simulator

**Table 4-2.** Zone 1 Stripping Efficiencies ( $\eta_1$ )

Expt. #	Liquid Flowrate (L/min)	Wind Speed (m/s)	Stripping Efficiencies (%)				
			Acetone	Ethyl Acetate	Toluene	Ethylbenzene	Cyclohexane*
S1	3.8	0	1.3	0.9	18.1	19.5	24.5
S2	7.6	0	0.3	ND	6.4	8.4	23.2
S3	7.6	1.62	0.7	0.4	8.5	9.6	26.4
S4	7.6	2.75	1.1	0.8	11.2	12.3	29.4
S5	11.4	0	ND	ND	3.6	4.2	12.5
S6	15.1	0	0.2	ND	3.5	4.1	12.3
S7	15.1	2.73	0.2	ND	3.2	3.7	14.8

\* = Values for cyclohexane include both zone 1 and zone 2 effects  
 ND = not determined

**Table 4-3.** Stripping Efficiencies Due to Surface Volatilization in a Trap ( $\eta_s$ )

Expt. #	Liquid Flowrate (L/min)	Wind Speed (m/s)	Stripping Efficiencies (%)			
			Acetone	Ethyl Acetate	Toluene	Ethylbenzene
S1	3.8	0	1.3	0.8	13.0	15.0
S2	7.6	0	0.3	n	2.5	5.0
S3	7.6	1.62	0.7	0.3	4.8	6.5
S4	7.6	2.75	1.0	0.7	7.1	8.7
S5	11.4	0	n	n	3.2	3.8
S6	15.1	0	0.1	n	2.2	2.9
S7	15.1	2.73	0.2	n	1.9	2.7

n =  $\eta_b > \eta_2$  (negative result)

During experiments with an intact falling film, measured stripping efficiencies also decreased slightly with increasing flowrate. While the air entrainment rate increased sharply between 11.4 and 15.1 L/min, the falling film associated with the lower flowrate was observed to have a more irregular appearance. It is possible that ventilation induced by this rougher film counteracted any emission reductions caused by the lower entrainment rate.

As with liquid flowrate, the wind speed passing over the drain hub had a variable effect on above-trap stripping efficiencies. During experiments with a disintegrated falling film there was a positive relationship between wind speed and both  $\eta_1$  and  $\eta_s$  (S2 to S4). It is possible that the presence of wind increased the amount of air exchange that occurred between the drain throat and the ambient atmosphere. It is also possible that mass transfer coefficients ( $K_L A_s$ ) themselves were affected by wind. During experiments with a disintegrated falling film, the wind was often observed to visibly distort and disperse the liquid film, in some cases altering its path to such a degree that the discharge nozzle had to be realigned. Further analysis would be necessary to determine whether wind increases stripping by means of ventilation, changes in  $K_L A_s$  or a combination of these effects.

As opposed to the disintegrated film, tracer stripping efficiencies associated with intact films exhibited virtually no changes when subjected to wind. As shown in Table 4-2, measured zone 1 stripping efficiencies for toluene and ethylbenzene in Experiments S6 and S7 were so similar that any deviations between them could reasonably be attributed to experimental error.

Additional experiments would be required to ascertain the mechanistic response of zone 1 stripping efficiencies to changes in wind speed for different liquid flow regimes. Such experiments were beyond the scope of this study.

Comparing the results in Tables 4-2 and 4-3, it appears that both air entrainment and surface volatilization are both important mechanisms for mass transfer in water seals. In most cases surface volatilization accounted for greater than 50% of total stripping. This finding is in contrast to the common assumption that all mass transfer in a water seal is attributable to air entrainment. This assumption is often based on a common view that when a jet impinges upon a liquid surface, entrained air is responsible for the vast majority of mass transfer, with the falling film contributing less than 1%, and surface volatilization constituting several percent at most (Bin, 1993). Among systems involving both air entrainment and surface volatilization, only one study could be found which attributed a majority (60%) of the oxygen mass transfer to surface volatilization, and this was for high energy surface aerator systems (Eckenfelder *et al.*, 1967).

#### **Correlations: Mass Transfer Parameters for Zone 1**

Empirical correlations were developed for the four parameters experimentally determined for zone 1:  $Q_e$ ,  $\gamma$ ,  $k_l A_s$ , and  $k_g A_s$ . Unlike mass transfer parameters, temperature was not expected to significantly affect  $Q_e$ . However, process flow velocity was considered an important variable as it was directly related to the momentum of the gaseous boundary layer which accompanies the falling film. The diameter of the nozzle was also considered an important parameter; assuming a constant thickness, the volume of the gaseous boundary layer is directly proportional to the film perimeter (for a circular film cross-section).

A total of 40 experiments were completed with trap simulators in an effort to measure the volumetric rate at which air is entrained within a water seal. Measured air entrainment rates for disintegrated and intact falling films are presented on Figures 4-1 and 4-2.

With both the disintegrated and intact falling films, there was a positive correlation between the liquid flowrate and the air entrainment rate. However, while the disintegrated relationship appeared to be linear, the relationship for the intact film more closely resembled an exponential function. For a given discharge nozzle diameter, increases in the liquid flowrate

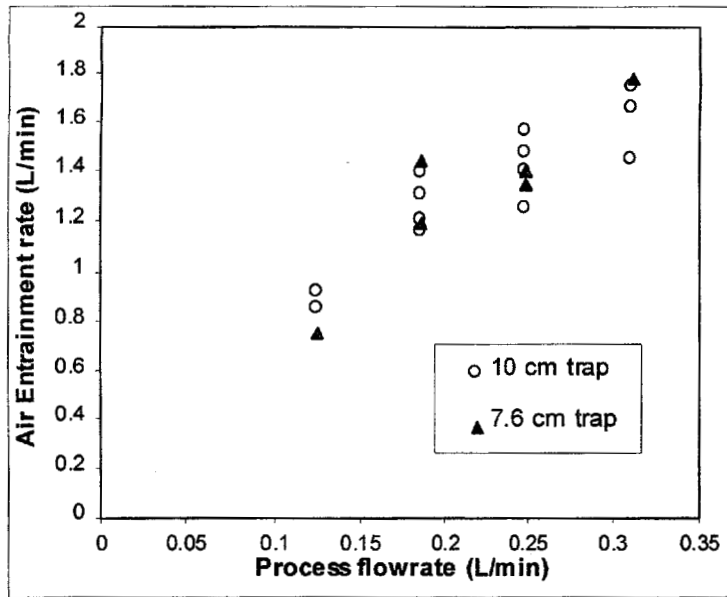


**Figure 4-1.** Air Entrainment Rates Measured with Disintegrated Liquid Flows

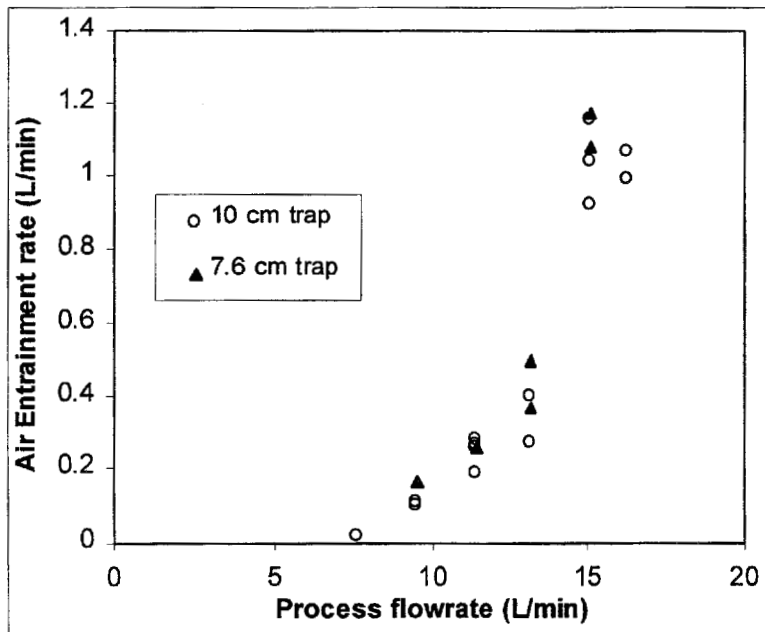


**Figure 4-2.** Air Entrainment Rates Measured with Intact Liquid Flows

increased both the velocity of the falling film and that of the gaseous boundary layer which accompanies it. However, within the disintegrated flow regime, higher flowrates were also characterized by a less dispersed film, i.e., one with a lower surface-to-volume ratio. These two effects tended to counteract one another, resulting in a weaker  $Q_e$  dependence upon liquid flowrate. Among intact flows, the physical appearance of the falling film was much less affected by increased process flow; thus, liquid velocity effects were more pronounced. Figures 4-1 and 4-2 indicate that the effects of trap diameter were negligible, at least between the 7.6 and 10 cm diameter traps.

Based on the reasoning and experimental results described above, the following empirical formulation was assumed for  $Q_e$ :

$$Q_e = \beta V_o^\omega d_o \quad (4-1)$$

where:

- $Q_e$  = air entrainment rate ( $L^3/T$ )
- $V_o$  = liquid velocity exiting drain nozzle ( $L/T$ )
- $d_o$  = nozzle diameter (L)
- $\beta, \omega$  = empirical constants (-)

Taking the logarithm of Equation 4-1 results in the following expression:

$$\log(Q_e) = \omega \log(V_o) + \log(\beta) + \log(d_o) \quad (4-2)$$

Using results from the entrainment experiments (10 cm diameter trap), a plot was drawn relating  $\log(Q_e)$  to  $\log(V_o)$ . Performing a linear regression on these data resulted in a best-fit line, the slope of which was equal to the fitting constant,  $\omega$ . To determine  $\beta$ , the logarithm of the nozzle diameter (0.0254 m) was subtracted from the y-intercept of this same best fit line.

$$Q_e = 135V_o^{0.63} d_o \quad (R^2 = 0.84, \text{ for disintegrated flows}) \quad (4-3)$$

$$Q_e = 1210V_o^{5.09} d_o \quad (R^2 = 0.94, \text{ for intact flows}) \quad (4-4)$$

where:

- $Q_e$  = air entrainment rate (L/min)
- $V_o$  = liquid velocity exiting drain nozzle (m/s)
- $d_o$  = nozzle diameter (m)

Confirming the trends observed on Figures 4-2 and 4-3, the intact flow correlation exhibited a stronger dependence on the liquid flowrate than did the correlation for disintegrated flow conditions. Although entrainment rates were typically larger for disintegrated process flows, the coefficient in Equation 4-3 is smaller than the one in Equation 4-4. Because the liquid velocities in this study were all significantly less than 1 m/s, the large exponent in Equation 4-4 resulted in much smaller calculated  $Q_e$  values.

In addition to the rate of bubble entrainment, the effects of entrained air on chemical emissions from water seals requires knowledge of the degree of equilibrium ( $\gamma$ ) achieved by bubbles prior to their ascent to the surface of the water seal. Equation 3-13 was used to determine values of  $\gamma$  for all B-series experiments. Results are presented in Table 4-4. As expected,  $\gamma$  was observed to be a strong function of Henry's law constant, decreasing as Henry's law constant increased. Correlations for  $\gamma$  were developed assuming that Henry's law constant, air entrainment rate, and liquid flow regime (disintegrated or intact) were important factors. Correlations for both liquid flow regimes were assumed to have the following form:

$$\gamma = 1 - a \cdot e^{-\frac{b}{Q_e H_c}} \quad (4-5)$$

where:

- $\gamma$  = degree of equilibrium (-)
- $Q_e$  = air entrainment rate ( $L^3/T$ )
- $H_c$  = Henry's law constant ( $L^3_{liq}/L^3_{gas}$ )
- $a, b$  = empirical constants (-)

Equation 4-5 is similar in form to an expression for mass transfer to a rising bubble (Roberts *et al.*, 1984). However, the phenomenon of mass transfer to air bubbles in an industrial process drain is significantly different from that in a quiescent liquid. For example, the

number of bubble circulations (passes) in a water seal may be different than the single and unimpeded trajectory in a quiescent fluid. Furthermore, Roberts *et al.* (1984) assumed a single bubble size as opposed to a size distribution that is likely more relevant for bubbles in a water seal. In Equation 4-5, "a" represents an empirical adjustment for the bubble size distribution effects, while "b" represents an adjustment for the number of circulations. Alternatively, "b" can be thought of as an "effective" mass transfer coefficient due to air entrainment.

Correlations for  $\gamma$  are shown below along with corresponding  $R^2$  values from the logarithmic best-fit analysis used to determine "a" and "b":

$$\gamma = 1 - 0.979 \left\{ e^{-\frac{0.309}{Q_e H_c}} \right\} \quad (\text{disintegrated flow, } R^2 = 0.93) \quad (4-6)$$

$$\gamma = 1 - 0.956 \left\{ e^{-\frac{0.123}{Q_e H_c}} \right\} \quad (\text{intact flow, } R^2 = 0.85) \quad (4-7)$$

where:

- $\gamma$  = degree of equilibrium (-)
- $H_c$  = Henry's law constant ( $L^3_{\text{liq}}/L^3_{\text{gas}}$ )
- $Q_e$  = air entrainment rate (liters/min)

Interestingly, the adjustment for bubble size distribution was very similar for both disintegrated and intact flows. The effective mass transfer coefficient for disintegrated flows was a factor of approximately 2.5 times greater than for intact flows.

Values of  $K_L A_s$  were determined by applying Equations 3-14 and 3-15 for S-series experiments. Corresponding results are listed in Table 4-5. As expected, values of  $K_L A_s$  increased with increasing Henry's law constant due to a reduction in gas-phase resistance to mass transfer. Values of  $K_L A_s$  for acetone and ethyl acetate are subject to greater uncertainty than those for toluene and ethylbenzene as they stem from the difference between two small numbers ( $\eta_1 - \eta_b$ ) in Equation 3-14. The range of  $K_L A_s$  was relatively small for all chemical tracers.

**Table 4-4.** Measured Degrees of Equilibrium ( $\gamma$ ) for Entrained Bubbles

Expt. #	Liquid Flowrate (L/min)	Degree of Equilibrium (-)				
		Acetone	Ethyl Acetate	Toluene	Ethylbenzene	Cyclohexane
B1	7.6	1.0	1.0	0.82	0.61	0.10
B2	9.5	1.0	1.0	0.80	0.59	0.09
B3	11.4	1.0	1.0	0.80	0.57	0.15
B4	15.1	1.0	1.0	0.75	0.56	0.08
B5	5.7	1.0	0.90	0.71	0.51	0.06
B6	7.6	0.91	0.85	0.77	0.55	0.10
B7	9.5	1.0	1.0	0.75	0.54	0.08
B8	11.4	0.49	1.0	0.71	0.54	0.06
B8-B	11.4	1.0	1.0	0.84	0.63	0.10
B9	15.1	0.99	1.0	0.68	0.52	0.06
B9-B	15.1	1.0	1.0	0.86	0.65	0.15
B10	5.7	0.91	1.0	0.54	0.35	0.03
B11	7.6	1.0	1.0	0.52	0.47	0.05
B12	9.5	1.0	0.87	0.79*	0.56	0.08
B13	11.4	0.96	0.97	0.57	0.37	0.06
B14	15.1	0.81	0.90	0.72	0.51	0.09
B14-B	15.1	0.98	1.0	0.69	0.51	0.08

B1-B4 = 5 cm trap simulator  
 B5-B9B = 7.6 cm trap simulator  
 B10-B14B = 10 cm trap simulator

Values of  $K_L A_s$  were used to determine liquid and gas-phase mass transfer coefficients ( $k_L A_s$  and  $k_g A_s$ ) using the residuals matrix method described in Chapter 3. Attempts were made to correlate values of  $k_L A_s$  and  $k_g A_s$  to several variables, including process flow rates, liquid velocities, liquid temperature, liquid and gas-phase Schmidt numbers, and liquid flow regime. Within the range of conditions tested for this study, only the liquid flow regime appeared to have an influence on  $k_L A_s$  and  $k_g A_s$ . Therefore, the following average values are recommended:

$$k_L A_s = 0.68 \cdot \left\{ \frac{D_{li}}{D_{li,EB}} \right\}^n \quad (\text{disintegrated}) \quad (4-8)$$

$$k_L A_s = 0.49 \cdot \left\{ \frac{D_{li}}{D_{li,EB}} \right\}^n \quad (\text{intact}) \quad (4-9)$$

$$k_g A_s = 37 \cdot \left\{ \frac{D_{gi}}{D_{g,ace}} \right\}^m \quad (\text{disintegrated}) \quad (4-10)$$

$$k_g A_s = 17 \cdot \left\{ \frac{D_{gi}}{D_{g,ace}} \right\}^m \quad (\text{intact}) \quad (4-11)$$

where:

- $k_l A_s$  = liquid-phase mass transfer coefficient (liters/min)
- $k_g A_s$  = gas-phase mass transfer coefficient (liters/min)
- $D_{li}$  = liquid-phase molecular diffusion coefficient for chemical i ( $L^2/T$ )
- $D_{l,EB}$  = liquid-phase molecular diffusion coefficient for ethylbenzene ( $L^2/T$ )
- $D_{gi}$  = gas-phase molecular diffusion coefficient for chemical i ( $L^2/T$ )
- $D_{g,ace}$  = gas-phase molecular diffusion coefficient for acetone ( $L^2/T$ )
- $n, m$  = power constants varying from 0.5 to 1.0 (-)

A discussion of the logic behind the bracketed terms in Equations 4-8 through 4-11 is provided in Chapter 2 of this report.

**Table 4-5.** Calculated Values of  $K_L A_s$

Expt. #	Liquid Flowrate (liters/min)	Wind Speed (m/s)	$K_L A_s$ (liters/min)			
			Acetone	Ethyl Acetate	Toluene	Ethylbenzene
S1	3.8	0	0.05	0.03	0.65	0.76
S2	7.6	0	0.03	0.0	0.21	0.43
S3	7.6	1.62	0.05	0.02	0.42	0.57
S4	7.6	2.75	0.08	0.06	0.64	0.78
S5	11.4	0	n	n	0.38	0.45
S6	15.1	0	0.02	n	0.34	0.47
S7	15.1	2.73	0.03	n	0.30	0.42

n = not listed due to values being negative

## Zone 2

### Experimental Results: Stripping Efficiencies

Within the underlying conveyance channel, the effects of air entrainment and surface volatilization were lumped together as one mechanism. Stripping efficiencies for each tracer in zone 2 ( $\eta_2$ ) were determined through the use of Equation 3-3. Figure 4-3 illustrates a typical data plot used to determine  $\eta_2$ . Similar plots were developed for each tracer. The time axis of these plots was shifted such that the time of the initial liquid sample, when  $-\ln(C_i/C_{i0}) = 0$ , corresponded to the y-intercept of the curve.

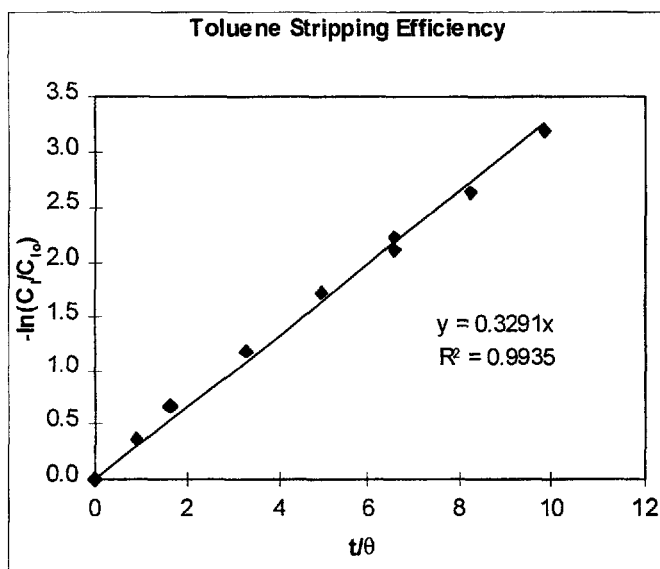


**Figure 4-3.** Toluene Stripping Efficiency for Experiment C5

Generally, the plots for toluene, ethylbenzene and cyclohexane resembled the one on Figure 4-3. However, for acetone and ethyl acetate the plots were often characterized by a high degree of variability and significantly lower coefficients of determination. This is related to the low Henry's law constant of these compounds; observed stripping was so minor that small chromatographic peak variations resulted in large relative differences in values of  $-\ln(C_i/C_{i0})$ . In one zone 2 experiment (C9) the toluene, ethylbenzene, and cyclohexane curves were observed to "flatten out." These results were due to an approach to chemical equilibrium in the channel headspace due to a reduction in the ventilation rate caused by the presence of a J-trap.

Stripping efficiencies associated with zone 2 experiments are presented in Table 4-6. Stripping efficiencies exhibited a strong dependence on Henry's law constant. Over all experimental conditions, measured stripping efficiencies ranged from 0.1% for acetone and ethyl acetate to 45% for cyclohexane. As with the zone 1 LDS experiments, measured stripping efficiencies for toluene and ethylbenzene were nearly identical, reflecting their similar physicochemical properties and serving as internal confirmation of experimental quality.

As with previously reported values, measured fractional stripping efficiencies were always higher when the falling film was disintegrated (C1 through C2B, C5 and C6). Within both the disintegrated and intact flow regimes,  $\eta_2$  decreased with increasing process flow.

A higher liquid temperature (33.1 °C) during Experiment C5 resulted in markedly higher stripping efficiencies relative to the otherwise identical Experiments C2 and C2-B. By elevating Henry's law constants and gas- and liquid-phase molecular diffusion coefficients, high temperatures tend to increase volatilization. At elevated temperatures, even acetone and ethyl acetate, whose measured  $\eta_2$  values were often near zero, were stripped in easily measurable quantities. It should also be noted that ventilation rates were higher for Experiment C5 than for Experiments C2 and C2-B. Thus, buoyancy induced air flow may have also contributed to larger stripping efficiencies.

During experiments where the hub was misaligned, the relationship between flowrate and stripping efficiency was weak. Experiment C6 was performed at 7.6 L/min, a normally disintegrated flowrate, while C7 was completed at 15.1 L/min, an intact flowrate. However, the differences in measured stripping efficiencies were not nearly as pronounced as those observed during aligned open drain experiments. Upon striking the hub, the falling films appeared very similar, both adhering to the walls of the drain throat and entering the channel in a similar fashion. Differences in  $\eta_2$  may have been due to the variable thickness of the liquid layer coating the drain throat walls, and the associated surface-to-volume ratio.

Experiment C8 was completed with a virtually empty channel, i.e., consistent with terminal drains. This led to increases in stripping efficiencies for acetone and ethyl acetate and slight decreases in the stripping efficiencies for the more volatile tracers.

**Table 4-6. Measured Stripping Efficiencies for Channel ( $\eta_2$ )**

Expt. #	Liquid Flowrate (L/min)	Liquid Temperature (°C)	Configuration	Stripping Efficiency (%)				
				Acetone	Ethyl Acetate	Toluene	Ethylbenzene	Cyclohexane
C1	3.8	21.7	open	2.0	4.5	30	31	45
C2	7.6	21.7	open	0.7	1.1	24	25	38
C2-B	7.6	23.9	open	0.8	1.9	26	27	40
C3	11.4	20.6	open	0.3	0.6	12	13	22
C4	15.1	20.4	open	0.5	0.4	8.2	8.6	18
C5	7.6	33.1	open	2.0	4.6	33	34	45
C6	7.6	20.1	open/misaligned	0.8	2.3	25	25	29
C7	15.1	21.8	open/misaligned	0.6	1.3	19	19	23
C8	7.6	20.0	open/empty channel	2.1	3.1	21	22	31
C9	7.6	19.7	trapped	0.6	0.1	2.7	3.3	17
C10	11.4	24.8	trapped	0.1	1.1	20	21	30
C11	15.1	24.5	trapped	0.6	10.	16	16	24

Zone 2 stripping efficiencies with a trapped drain in place were evaluated during Experiments C9 through C11. The most striking trend was the large increase in the stripping which occurred between Experiments C9 and C10. This was caused by the forced ventilation that was introduced into the channel during Experiments C10 and C11. It is believed that most of the difference in the measured stripping efficiency was due to an increase in the concentration driving force; tracers were swept from the channel headspace before they could accumulate and impede mass transfer. Increased ventilation may also increase the gas-phase mass transfer coefficient.

**Correlations: Mass Transfer Parameters**

Overall mass transfer coefficients for the underlying channel ( $K_L A_c$ ) were determined by using an iterative technique and Equations 3-4 through 3-8 (see Chapter 3). Results are presented in Table 4-7.

**Table 4-7.** Calculated Values of  $K_L A_c$

Expt. #	Overall Mass Transfer Coefficient					
	Liquid Flowrate (L/min)	Acetone (L/min)	Ethyl Acetate (L/min)	Toluene (L/min)	Ethylbenzene (L/min)	Cyclohexane (L/min)
C1	3.8	0.21	0.32	1.75	1.80	2.97
C2	7.6	0.14	0.12	2.66	2.80	4.85
C2-B	7.6	0.12	0.23	3.07	3.18	5.28
C3	11.4	0.01	0.16	1.69	1.78	3.42
C4	15.1	0.46	0.69	4.14	4.28	6.59
C5	7.6	0.06	0.10	1.74	1.86	3.25
C6	7.6	0.13	0.36	2.87	2.86	3.23
C7	15.1	0.75	0.54	4.38	5.07	4.91
C8	7.6	-	2.02	2.36	2.37	3.56
C9	7.6	0	0.10	0.81	0.88	2.80
C10	11.4	0.1	0.34	3.56	3.65	4.09
C11	15.1	0	0.45	3.69	3.73	4.84

Measured  $K_L A_c$  values from experiments involving disintegrated flow (C1, C2, C2-B) varied over a wider range than those associated with intact flows (C3, C4). Within each range, the relationship between  $K_L A_c$  and liquid flowrates was substantially different. Values of  $K_L A_c$  increased sharply between 3.8 and 7.6 L/min (disintegrated flows). However, during experiments with intact process flows,  $K_L A_c$  remained fairly constant.

Values of  $K_L A_c$  were observed to increase with increasing Henry's law constants, suggesting that gas-phase resistance to mass transfer was important for all compounds, with the possible exception of cyclohexane. Values of  $K_L A_c$  for toluene and ethylbenzene were very similar.

Compared to aligned and open process drains, drains in which the process flow was misaligned (Experiments C6 and C7) were characterized by significantly larger gas-phase mass transfer coefficients. This was probably due to the large interfacial area of the process flow as it adhered to the drain throat walls. This large area resulted in noticeably higher ventilation rates within the channel headspace. This larger  $k_g A_c$  also explains the weaker relationship between  $K_L A_c$  and  $H_c$  observed during Experiments C6 and C7; larger  $k_g A_c$  values act to reduce gas-phase resistance to mass transfer, thus lessening the importance of the Henry's law constant. Interestingly, the liquid-phase mass transfer coefficient was only marginally affected by a misaligned flow.

Experiment C8 was completed with an empty sewer reach. This condition resulted in lower liquid phase mass transfer coefficients and higher gas-phase mass transfer coefficients when compared to other open drain experiments, where the channel was approximately 20% full.

Values of  $k_f A_c$  and  $k_g A_c$  were determined through the use of Equations 3-9 through 3-11 and the residuals matrix method described in Chapter 3. This approach involved the determination of optimal values of  $k_g/k_f$  to provide best fits between the measured and predicted ratios of overall mass transfer coefficients for all tracer combinations. Measured values of  $k_g/k_f$  are listed in Table 4-8 for all C-series experiments.

During open drain experiments very similar to C2 through C4, Shepherd (1996) reported  $k_g/k_f$  ratios between 1 and 10. For this study, experiments characterized by large ventilation rates (C6, C7, C10, C11) were also characterized by large  $k_g/k_f$  ratios, possibly due to increases in the gas-phase mass transfer coefficient. These values were roughly consistent with those presented by other authors; Hsieh *et al.* (1991) reported  $k_g/k_f$  ratios between 38 and 110 for surface-agitated systems, while Munz and Roberts (1989) recommended a value of 40 for modeling surface aerators.

**Table 4-8.** Measured  $k_g/k_l$  Ratios for the Underlying Sewer Channel (zone 2)

Expt. #	Experimental Conditions	$k_g/k_l$
C1	open drain	41
C2	open drain	7.5
C2-B	open drain	12
C3	open drain	9.3
C4	open drain	11
C5	open drain, high $T_{lg}$	23
C6	misaligned hub	29
C7	misaligned hub	32
C8	empty channel	2.3
C9	J-trap	1.7
C10	J-trap, forced ventilation	17
C11	J-trap, forced ventilation	21

Experiments C9, C10 and C11 were completed to quantify the mass transfer which occurs in the channel below a water seal. The large differences in  $K_L A_c$  and  $k_g/k_l$  between Experiments C9 and C10 were due to the forced ventilation which was conducted during Experiments C10 and C11.

Liquid temperature had a substantial effect on the amount of mass transfer which occurred within the channel. Stripping efficiencies and overall mass transfer coefficients were all large during Experiment C5, when the process temperature was an elevated 33.1 °C. Within the correlations presented below, temperature effects were incorporated into the liquid-phase and gas-phase Schmidt numbers.

Attempts were made to correlate  $k_l A_c$  and  $k_g A_c$  to several experimental variables. Within the range of experimental conditions, the following correlations were determined to be the most appropriate:

$$k_l A_c = 205V_o^{-0.938} Sc_l^{-1/2} \text{ (sealed drain, } R^2 = 0.81) \tag{4-12}$$

$$k_l A_c = \{-1350 (V_o - 0.249)^2 + 149.5\} Sc_l^{-1/2} \text{ (open drain, } R^2 = 0.69) \tag{4-13}$$

$$k_g A_c = 3240V_o^{4.26} Sc_g^{-2/3} \text{ (sealed drain } R^2 = 0.69) \tag{4-14}$$

$$k_{gs} A_c = 17.2 k_l A_c \text{ (open drain)} \tag{4-15}$$

where:

$k_l A_c$  = liquid-phase mass transfer coefficient for channel (liters/min)

$k_g A_c$  = gas-phase mass transfer coefficient for channel (liters/min)

$V_o$  = liquid velocity exiting drain nozzle (m/s)

$Sc_l$  = liquid-phase Schmidt number =  $v_w/D_{li}$  (-)

$Sc_g$  = gas-phase Schmidt number =  $v_a/D_{gi}$  (-)

$v_w$  = kinematic viscosity of water ( $L^2/T$ )

$v_a$  = kinematic viscosity of air ( $L^2/T$ )

$D_{li}$  = liquid-phase molecular diffusion coefficient for chemical i ( $L^2/T$ )

$D_{gi}$  = gas-phase molecular diffusion coefficient for chemical i ( $L^2/T$ )

No consistent trends were observed for  $k_g A_c$  associated with open drains. Values of  $k_g/k_l$  ranged from 9.3 to 41 with an average of 17.2. Equation 4-15 is based on an arithmetic mean of  $k_g/k_l$  over all open drain experiments and, as such, does not include an  $R^2$  value.

Caution should be exercised when extrapolating Equations 4-12 through 4-15 beyond the range of experimental conditions from which they were developed. For example, values of  $k_l A_c$  for an open drain become negative for  $V_o > 0.58$  m/s. A conservative approach might be to use the  $k_l A_c$  value at  $V_o = 0.50$  m/s for all velocities greater than or equal to 0.50 m/s.

## 5. MODEL INTEGRATION AND APPLICATIONS

### SUMMARY OF EMISSIONS MODEL

The correlations described in Chapter 4 comprise an integrated model that can be used to predict VOC emissions from industrial process drains. Lists of relevant equations are provided in Table 5-1 (open drains) and Table 5-2 (trapped drains). For the latter it has been assumed that all drains would be trapped, such that minimal emissions would result from below the trap itself, i.e., from the underlying channel. A list of all relevant variables is provided in Table 5-3. In Chapter 4, units were often provided in generic form, e.g., L/T = length per unit time. Specific units have been provided for all variables in Table 5-3 in order to avoid confusion and to ensure that the requirement for consistent units is met.

**Table 5-1.** Summary of Model Equations for Open Drains

	Equation No.
$E = \eta_2 Q_i C_{i0}$	
$\eta_2 = 1 - \frac{(Q_i + Q_c) \left( \frac{Q_c C_{c0} + Q_i C_{i0} + \frac{K_L A_c Q_{gc} C_{gc}}{H_c Q_{gc} + H_c Q_{gd} + K_L A_c}}{Q_c + Q_i + K_L A_c - \frac{(K_L A_c)^2}{H_c Q_{gc} + H_c Q_{gd} + K_L A_c}} \right)}{Q_c C_{c0} + Q_i C_{i0}}$	(2-6)
$\frac{1}{K_L A_c} = \frac{1}{k_l A_c} + \frac{1}{k_g A_c H_c}$	(2-2)
$k_l A_c = \{-1350 (V_o - 0.249)^2 + 149.5\} Sc_l^{-1/2} \text{ (open drain, } R^2 = 0.69)$	(4-13)
$k_g A_c = 17.2 k_l A_c \text{ (open drain)}$	(4-15)

**Table 5-2.** Summary of Model Equations for Trapped Drains (with water seals)

	Equation No.
$E = \eta_1 Q_i C_{10}$	
$\eta_1 = 1 - \frac{1}{1 + \frac{Q_e}{Q_i} H_c \gamma + \frac{K_L A_s}{Q_i}}$	(2-5)
$Q_e = 135 V_o^{0.63} d_o \quad (R^2 = 0.84, \text{ for disintegrated flows})$	(4-3)
$Q_e = 1210 V_o^{5.09} d_o \quad (R^2 = 0.94, \text{ for intact flows})$	(4-4)
$\gamma = 1 - 0.979 \left\{ e^{-\frac{0.309}{Q_e H_c}} \right\} \quad (\text{disintegrated flow, } R^2 = 0.93)$	(4-6)
$\gamma = 1 - 0.956 \left\{ e^{-\frac{0.123}{Q_e H_c}} \right\} \quad (\text{intact flow, } R^2 = 0.85)$	(4-7)
$\frac{1}{K_L A_s} = \frac{1}{k_l A_s} + \frac{1}{k_g A_s H_c}$	(2-2)
$k_l A_s = 0.68 \bullet \left\{ \frac{D_{li}}{D_{l,EB}} \right\}^n \quad (\text{disintegrated})$	(4-8)
$k_l A_s = 0.49 \bullet \left\{ \frac{D_{li}}{D_{l,EB}} \right\}^n \quad (\text{intact})$	(4-9)
$k_g A_s = 37 \bullet \left\{ \frac{D_{gi}}{D_{g,ace}} \right\}^m \quad (\text{disintegrated})$	(4-10)
$k_g A_s = 17 \bullet \left\{ \frac{D_{gi}}{D_{g,ace}} \right\}^m \quad (\text{intact})$	(4-11)

**Table 5-3.** Description of Variables

VARIABLE	DESCRIPTION
$C_{co}$	upstream liquid channel concentration (mg/liter)
$C_{gc}$	upstream headspace gas concentration (mg/liter)
$C_{lo}$	liquid-phase concentration in process discharge to drain (mg/liter)
$d_o$	nozzle diameter (m)
$D_{gi}$	gas-phase molecular diffusion coefficient for compound i ( $m^2/s$ )
$D_{g,ace}$	gas-phase molecular diffusion coefficient for acetone ( $m^2/s$ )
$D_{li}$	liquid-phase molecular diffusion coefficient for chemical i ( $m^2/s$ )
$D_{l,EB}$	liquid-phase molecular diffusion coefficient for ethylbenzene ( $m^2/s$ )
$E$	process drain emission rate (mg/s)
$H_c$	Henry's law constant ( $m^3_{liq}/m^3_{gas}$ )
$k_g A_c$	gas-phase mass transfer coefficient for channel (liters/min)
$k_g A_s$	gas-phase mass transfer coefficient for water seal (liters/min)
$k_l A_c$	liquid-phase mass transfer coefficient for channel (liters/min)
$k_l A_s$	liquid-phase mass transfer coefficient for water seal (liters/min)
$K_L A_c$	overall mass transfer coefficient for channel (liters/min)
$K_L A_s$	overall mass transfer coefficient for surface volatilization (liters/min)
$n, m$	power constants varying from 0.5 to 1.0 (-)
$Q_c$	upstream liquid channel flowrate (liters/min)
$Q_e$	air entrainment rate (liters/min)
$Q_{gc}$	upstream headspace gas flowrate (liters/min)
$Q_{gd}$	gas flowrate drawn into process drain throat (liters/min)
$Q_l$	process flowrate into drain (liters/min)
$Sc_l$	liquid-phase Schmidt number = $\nu_w/D_{li}$ (-)
$V_o$	liquid velocity exiting drain nozzle (m/s)
$\eta_1$	fractional stripping efficiency for zone 1 (-)
$\eta_2$	fractional stripping efficiency for zone 2 (-)
$\gamma$	extent of chemical equilibrium in entrained bubbles (-)
$\nu_w$	kinematic viscosity of water ( $m^2/s$ )

### Comparison With Existing Models

The emissions model was compared to existing models designed to estimate VOC emission rates from industrial process drains. Trapped drain emissions were compared to those predicted from the USEPA model (WATER8) based on Enviromega's 1993 study (USEPA, 1994). Open drain emission rates were compared to predicted stripping efficiencies determined using BACT/LAER (USEPA, 1990).

Model comparisons were completed over a range of liquid flowrates and Henry's law constants. When adjusting system variables, a default set of standard conditions was applied. For this analysis, the standard process flow was a 7.6 L/min disintegrated film discharged from a 2.54 cm discharge nozzle. The process flow temperature was 25 °C. The ventilation rate in the channel was 40 L/min, and there was no wind. Toluene ( $H_c = 0.27 \text{ m}^3_{\text{liq}}/\text{m}^3_{\text{gas}}$  at 25 °C) was chosen as the default tracer.

Figure 5-1 illustrates the relationships between trapped drain stripping efficiencies and process flowrate.

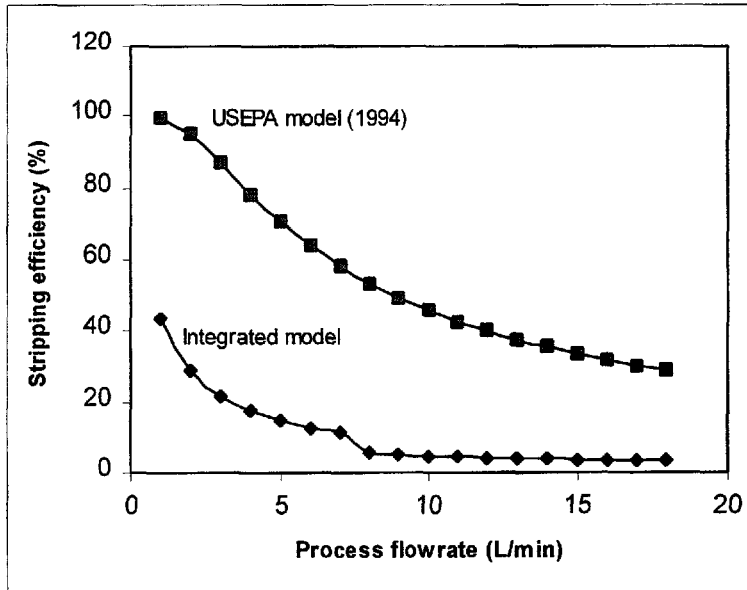


**Figure 5-1.** Integrated Model Compared with USEPA WATER8 Model (1994) (trapped drain, varying  $Q_i$ ).

Over the range of liquid flowrates that were applied, the USEPA model predicted substantially higher toluene stripping efficiencies. This was most noticeable at low process flows, where predicted stripping efficiencies from the USEPA model were over 99%. These extreme values were likely the result of the data set used to develop the USEPA model. During Enviromega's original studies, process flowrates of 0, 15 and 49 L/min were used. Presumably, only data from the latter two flowrates were utilized to determine a relationship between stripping efficiency and process flow. This finding is particularly important given the fact that most process drains are believed to operate at relatively low ( $\approx 4$  L/min) flowrates (American Petroleum Institute, 1996). The flowrates used in this study extended to as low as 3.8 L/min. On Figure 5-1, the change from disintegrated to intact flow occurred at 8 L/min and is reflected in a sudden decrease in stripping efficiency.

The two models were also compared over a range of Henry's law constants. This comparison is shown on Figure 5-2. For a given Henry's law constant the USEPA model always predicts a significantly higher stripping efficiency. As with the flowrate relationship, this was likely due to the limited data set used to develop the USEPA empirical correlations. Chemicals with Henry's law constants ranging from  $0.0015 \text{ m}^3_{\text{liq}}/\text{m}^3_{\text{gas}}$  to  $7.3 \text{ m}^3_{\text{liq}}/\text{m}^3_{\text{gas}}$  at  $25^\circ\text{C}$  were used in this study.

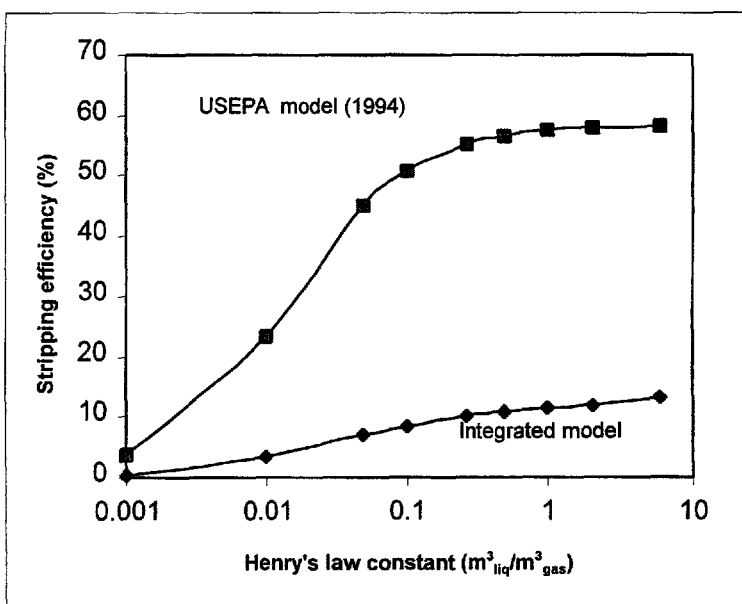


**Figure 5-2.** Integrated Model Compared with USEPA WATER8 Model (1994) (trapped drain, varying  $H_c$ )

For open drains, the model developed in this study was compared to BACT/LAER, an equilibrium-based emissions model. The results of this comparison are illustrated on Figure 5-3.

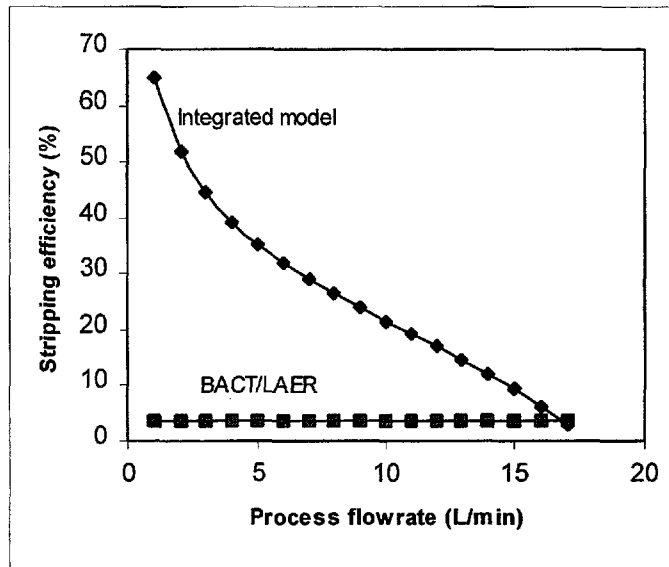


**Figure 5-3.** Integrated Model Compared with BACT/LAER (open drain, varying  $Q_i$ )

The BACT/LAER-predictions were independent of process flowrate; the stripping efficiency of toluene was fixed at 3.6%. Large channel stripping efficiencies predicted by the integrated model were due to the relatively high default ventilation rate (40 L/min).

The integrated model from this study was also compared to BACT/LAER over a range of Henry's law constants. This comparison is shown on Figure 5-4. The estimated BACT/LAER stripping efficiency exceeded 100% at an  $H_c$  value of approximately  $10 \text{ m}^3_{\text{liq}}/\text{m}^3_{\text{gas}}$ . The integrated model leads to higher predicted stripping efficiencies for  $H_c$  in the range of 0.01 to  $3 \text{ m}^3_{\text{liq}}/\text{m}^3_{\text{gas}}$ . Shepherd (1996) found that BACT/LAER underestimated stripping efficiencies for toluene ( $H_c = 0.27 \text{ m}^3_{\text{liq}}/\text{m}^3_{\text{gas}}$  at  $25^\circ\text{C}$ ) and overestimated stripping efficiencies for cyclohexane ( $H_c = 7.3 \text{ m}^3_{\text{liq}}/\text{m}^3_{\text{gas}}$  at  $25^\circ\text{C}$ ). This observation agrees with Figure 5-4 as well as with channel stripping efficiencies measured in this study.

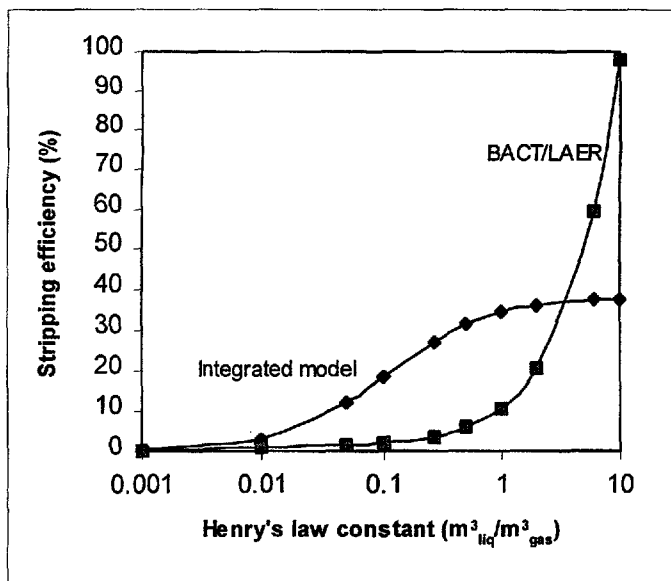


**Figure 5-4.** Integrated Model Compared with BACT/LAER (open drain, varying  $H_c$ )

Figures 5-3 and 5-4 illustrate the effects of varying process flowrates and Henry's law constant at otherwise "standard" conditions for an open drain. Another important parameter for open drains is the extent to which the drain is ventilated, i.e., rate of air movement through the drain throat. To illustrate the effects of drain throat ventilation, the standard conditions described previously were employed (toluene at 25 °C; liquid process flowrate = 7.6 L/min; nozzle diameter = 2.54 cm). Channel flow and upstream channel air flow were assumed to be negligible. It was further assumed that the drain throat was ventilated by an ingassing (co-current) air flowrate that was allowed to vary from 0 L/min (which leads to zero stripping) to 100 L/min.

Results are provided on Figure 5-5, which illustrates the importance of air exchange rates through process drains ( $Q_{gd}$  in Equation 2.6) on stripping efficiency. The relationship between stripping efficiency and  $Q_{gd}$  is nearly linear at low values of  $Q_{gd}$  and approaches a constant value at high values of  $Q_{gd}$ . This latter condition corresponds to an approach to infinite ventilation, i.e., completely open/exposed drain and underlying channel, and provides an upper-bound estimate of stripping efficiencies for open drains.

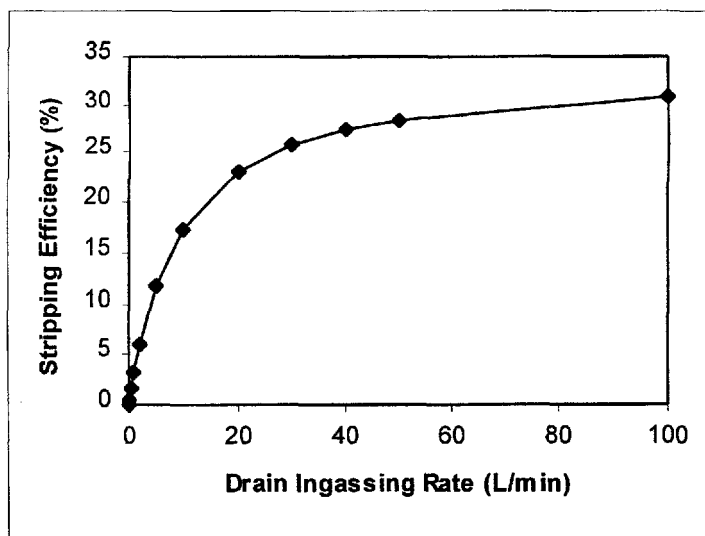


**Figure 5-5.** Toluene Stripping Efficiency Versus Drain Ingassing Rate for an Open Drain

Finally, the integrated model can be used to estimate the effects of placing water seals on existing open drains. As an example, the following open drain conditions were assumed: liquid process flowrate = 7.6 L/min (disintegrated), temperature = 25 °C, nozzle diameter = 2.54 cm, no channel liquid or gas flowrates upstream of drain, drain ingas rate = 10 L/min. For these conditions, the stripping efficiencies for three different chemicals with Henry's law constants equal to  $0.05 \text{ m}^3_{\text{liq}}/\text{m}^3_{\text{gas}}$ ,  $0.27 \text{ m}^3_{\text{liq}}/\text{m}^3_{\text{gas}}$  (e.g., toluene) and  $7 \text{ m}^3_{\text{liq}}/\text{m}^3_{\text{gas}}$  (e.g., cyclohexane) were 5.1%, 13%, and 37%, respectively. If a water seal is added to the drain the predicted stripping efficiencies change to 7% (from 5.1%), 10% (from 13%), and 14% (from 37%). For these hypothetical conditions, the addition of a water seal would reduce emissions of the most volatile chemical by 62%. Emissions of the mid-volatility chemical would be reduced only slightly, i.e., by 23%. However, for the same hypothetical conditions, emissions of the lower-volatility chemical would actually increase by approximately 40% when a water seal is added. Because the model is non-linear, there are certain combinations of hydrodynamic conditions and chemical properties that can lead to higher predicted emissions when a seal is placed in a drain. These results apply to a single drain in isolation of the remainder of the sewer network. Results could vary if the entire network is considered.

The example results described above would change as operating conditions are changed, and there are certainly some scenarios in which the use of water seals can lead to substantial reductions in VOC emissions. The analysis provided herein is intended to

demonstrate the utility of an integrated mechanistic model for predicting VOC emissions and for identifying those conditions for which passive control strategies, e.g., water seals, are either viable or detrimental.

## 6. SUMMARY AND CONCLUSIONS

### SUMMARY

A two-zone emissions model was developed for estimating VOC emissions from refinery process drains. The model includes estimates of emissions from a water seal (zone 1) and an underlying channel (zone 2). For zone 1, the model includes estimates of air entrainment, degree of chemical equilibrium between entrained air bubbles and surrounding liquid, and gas- and liquid-phase mass transfer coefficients associated with volatilization across the upstream surface of a water seal. For zone 2, the model includes estimates of gas- and liquid-phase mass transfer coefficients in the channel below an active process drain.

Five volatile tracers and two separate experimental drain systems were used to develop model parameters. A total of 76 experiments were completed with the two experimental systems.

Chemical stripping efficiencies, rate of air entrainment, degrees of chemical equilibrium for entrained bubbles, and overall mass transfer coefficients for channels and traps were presented in Chapter 4. A discussion of experimental results was provided. Correlations were developed for all relevant mass transfer parameters. These correlations then served as part of an integrated emissions model that was presented in Chapter 5. Several model applications were presented, particularly as related to comparing the results of this study to those based on predictions resulting from existing emissions models. Significant differences were observed for emissions estimates based on the model developed from this study and those based on existing models. The utility of the model developed for this study as a means for predicting the effectiveness of water seals was also described in Chapter 5.

### CONCLUSIONS

Specific conclusions that resulted from this study are listed below:

1. Stripping efficiencies in water seals increase with increasing Henry's law constant and may approach 20% at moderate liquid temperatures (20° to 30 °C) for chemicals with Henry's law

constants similar to or greater than toluene. However, stripping efficiencies for lower-volatility chemicals, e.g., acetone and ethyl acetate, should generally be on the order of 1% or lower.

2. Both air entrainment and surface volatilization are important contributors to mass transfer at water seals. For this study, the effects of surface volatilization were generally greater than those associated with entrained air.
3. Stripping efficiencies in water seals decrease substantially as the jet that impinges on the seal moves from a disintegrated film to a solid (intact) film. This is generally due to the effects of similar air entrainment rates but longer hydraulic residence times for the lower flows associated with disintegrated films.
4. Wind speed above a drain hub affects VOC emissions from drains with disintegrated process flows. However, the effects of wind on intact process flows appear to be small. The specific mechanism by which wind affects emissions during disintegrated flow conditions was not determined but could include increases in mass transfer coefficients, increases in interfacial area due to distortion of the falling film, increased ventilation of the drain throat, or some combination of the above.
5. Air entrainment rates in a water seal are significantly influenced by, and increase with, increases in process flowrate. Entrainment rates do not appear to be significantly influenced by the diameter of a drain throat or corresponding water seal.
6. The degree of chemical equilibrium between entrained air bubbles and surrounding liquid is highly dependent on Henry's law constant, and is also affected by changes in air entrainment rate. The degree of equilibrium increases with decreases in Henry's law constant and entrainment rate. It is reasonable to assume that chemicals with Henry's law constants as low as ethyl acetate and acetone will have a degree of equilibrium that approaches unity. However, highly volatile chemicals, e.g., cyclohexane or 1,3-butadiene, should have degrees of equilibrium that are generally less than 0.1 (10% of equilibrium). For these chemicals, an assumption of equilibrium for bubbles can lead to significant overestimation of emissions.
7. Stripping efficiencies associated with open drains are generally, but not always, greater than those for water seals for similar operating conditions. For this study, stripping efficiencies as high as 45% (cyclohexane) were observed for open drains.
8. Significant variations in stripping efficiency can occur as the operating conditions of open drains are varied. As with water seals, stripping efficiencies for open drains decrease as the process flow moves from being a disintegrated to a solid jet.

9. Elevated liquid temperatures can lead to substantial increases in chemical stripping efficiencies, particularly for lower-volatility chemicals. Increases in liquid temperature lead to increases in Henry's law constant, increases in mass transfer coefficients, and increases in buoyancy-induced ventilation.
10. The integrated two-zone model developed for this study should be a valuable tool for estimating VOC emissions from process drains. It is more mechanistic in nature than existing emissions models for process drains, and allows for an investigation of the effects of system operating conditions and chemical properties on VOC emissions.
11. An existing USEPA model (WATER8) may significantly overestimate stripping efficiencies, and subsequently emissions, from process drains that contain water seals.
12. Except in the case of highly-volatile chemicals, e.g., cyclohexane, BACT/LAER may underestimate VOC emissions and does not account for the mechanistic behavior of emissions as process operating conditions are varied.

## 7. REFERENCES

American Petroleum Institute, *Phase I report: Estimation of fugitive emissions from petroleum refinery process drains*, 1996. API Publication No. 4639.

Ashworth, R.A., Howe, G.B., Mullings, M.E., Rogers, T.N., "Air-water partitioning coefficients of organics in dilute aqueous solutions," *Journal of Hazardous Materials*, Vol. 18, 1988, pp. 25-36.

Berthouex, P.M., Brown, L.C., Statistics for Environmental Engineers, Lewis Publishers Inc., Boca Raton, FL, 1994.

Bin, A.K., "Gas entrainment by plunging liquid jets," *Chemical Engineering Science*, Vol. 48, No. 21, 1993, pp. 3585-3630.

Danckwerts, P.V., "Significance of liquid film coefficients in gas absorption," *Industrial and Engineering Chemistry*, Vol. 43, No. 6, 1951, pp. 1460-1467.

Dobbins, W.E., "The nature of the oxygen transfer coefficient in aeration systems," in Biological Treatment of Sewage and Industrial Waste, Volume 1, J. McCabe and W.W. Eckenfelder, Jr., eds., Chap. 2-1, Reinhold Publishing Corporation, New York, 1956, pp. 141-148.

Eckenfelder, W.W., Ford, D.L., "Engineering aspects of surface aeration design," *Proceedings of the 22<sup>nd</sup> Purdue Industrial Waste Conference*, 1967, Lafayette, IN.

Enviromega, Ltd., *Measurement of hazardous air pollutant emissions from wastewater collection system components, Volume II: Process drains*, 1993.

Fitzgerald, B.M., "Evaluation of adsorbents for the collection and analysis of vapors during radio frequency heating of fuel contaminated soil," Master's Report, The University of Texas at Austin, 1996.

Higbie, R., "The fate of exposure of a pure gas into a still liquid during short periods of exposure," *Transactions, Amer. Inst. of Chem. Engrs.*, Vol. 31, 1935.

Howard, C., Strader, R., and Corsi, R.L., "Improved estimation of chemical stripping from drinking water to indoor air," *Proceedings of the 89<sup>th</sup> Annual Meeting & Exhibition of the Air and Waste Management Association*, June 23-28, 1996, Nashville, TN.

Hsieh, C.-C., Ro, K.S., Stenstrom, M.K., "Estimating stripping rates and gas-liquid mass transfer coefficients of semi-volatile organic compounds in surface aeration," *64<sup>th</sup> Annual Conference of the Water Pollution Control Federation*, October 6-10, 1991, Toronto, ON.

Hsieh, C.-C., Ro, K.S., Stenstrom, M.K., "Estimating semi-volatile organic compound emission rates and oxygen transfer coefficients in diffused aeration," *65<sup>th</sup> Water Environment Federation Conference*, September 20-24, 1992, New Orleans, LA.

Lewis, W.K., and Whitman, W.G., "Principles of gas absorption," *Industrial and Engineering Chemistry*, 16, 1215-1220 (1924).

Mackay, D., Yuen, A.T.K., "Mass transfer coefficient correlations for volatilization of organic solutes from water," *Environmental Science and Technology*, Vol. 17, No. 4, 1983, pp. 211-217.

Munz, C., Roberts, P.V., "Gas- and liquid-phase mass transfer resistances of organic compounds during mechanical surface aeration," *Water Research*, Vol. 23, No. 5, 1989, pp. 589-601.

Roberts, P.V., Munz, C., and Dandliker, P., "Modeling volatile organic solute removal by surface and bubble aeration," *Journal of Water Pollution Control Federation*, Vol. 56, No. 2, 1984, pp. 157-163.

Shepherd, J.L., "Mass transfer of volatile organic compounds at industrial process drains," Master's Thesis, The University of Texas at Austin, 1996.

Simes, G.F., *Preparation Aids for the Development of Category III Quality Assurance Project Plans*, EPA/600/8-91/005, Office of Research and Development, United States Environmental Protection Agency, Cincinnati, 1991.

Smith, J.M., Chemical Engineering Kinetics, Third ed., McGraw-Hill Book Company, New York, 1981.

USEPA, *Industrial wastewater volatile organic compound emissions – Background information for BACT-LAER determinations*. EPA-450/3-90-004, 1990.

USEPA, *Air emissions models for waste and wastewater*. EPA-453/R-94-080A (manual for WATER8 model), 1994.

Van de Sande, E., and Smith, J.M., "Surface entrainment of air by high velocity water jets," *Chemical Engineering Science*, Vol. 28, 1973, pp. 1161-1168.

Van de Sande, E., and Smith, J.M., "Mass transfer from plunging water jets," *The Chemical Engineering Journal*, Vol. 10, 1975, pp. 225-233.

Van de Sande, E., and Smith, J.M., "Jet break-up and air entrainment by low velocity turbulent water jets," *Chemical Engineering Science*, Vol. 31, 1976, pp. 219-224.

The American Petroleum Institute provides additional resources and programs to industry which are based on API Standards.

For more information, contact:

- Training and Seminars Ph: 202-682-8490  
Fax: 202-682-8222
- Inspector Certification Programs Ph: 202-682-8161  
Fax: 202-962-4739
- American Petroleum Institute  
Quality Registrar Ph: 202-962-4791  
Fax: 202-682-8070
- Monogram Licensing Program Ph: 202-962-4791  
Fax: 202-682-8070
- Engine Oil Licensing and  
Certification System Ph: 202-682-8233  
Fax: 202-962-4739
- Petroleum Test Laboratory  
Accreditation Program Ph: 202-682-8064  
Fax: 202-962-4739

In addition, petroleum industry technical, patent, and business information is available online through API EnCompass™. Call 212-366-4040 or fax 212-366-4298 to discover more.

To obtain a free copy of the API Publications, Programs, and Services Catalog, call 202-682-8375 or fax your request to 202-962-4776. Or see the online interactive version of the catalog on our World Wide Web site — <http://www.api.org>.



**American  
Petroleum  
Institute**

**Helping You  
Get The Job  
Done Right.**



**American  
Petroleum  
Institute**

0732290 0614797 912

1220 L Street, Northwest  
Washington, D.C. 20005  
202-682-8000  
<http://www.api.org>

***API'S RELATED PUBLICATIONS...***

- PUBL 4639 ESTIMATION OF FUGITIVE EMISSIONS FROM PETROLEUM REFINERY  
PROCESS DRAINS - PHASE I REPORT, APRIL 1996
- PUBL 4677 FUGITIVE EMISSIONS FROM REFINERY PROCESS DRAINS, VOLUME I:  
FUGITIVE EMISSION FACTORS FOR REFINERY PROCESS DRAINS,  
APRIL 1999
- PUBL 4681 FUGITIVE EMISSIONS FROM REFINERY PROCESS DRAINS, VOLUME III:  
PROCESS DRAIN EMISSION CALCULATOR (APIDRAIN), APRIL 1999

***To order, call API Publications Department (202) 682-8375***

Order No. I46780